FTPI-MINN-21-20, UMN-TH-4103/2, INR-TH-2021-021

Black hole induced false vacuum decay: The role of greybody factors

Andrey Shkerin[a*], Sergey Sibiryakov[b,c,d†]

[a] *William I. Fine Theoretical Physics Institute, School of Physics and Astronomy, University of Minnesota, Minneapolis, MN 55455, USA*

[b] *Department of Physics & Astronomy, McMaster University, Hamilton, Ontario, L8S 4M1, Canada*

[c] *Perimeter Institute for Theoretical Physics, Waterloo, Ontario, N2L 2Y5, Canada*

[d] *Institute for Nuclear Research of the Russian Academy of Sciences, 60th October Anniversary Prospect, 7a, 117312 Moscow, Russia*

arXiv:2111.08017v2 [hep-th] 22 Aug 2022

Abstract

We study false vacuum decay catalyzed by black holes. We consider a toy two-dimensional model of a scalar field with an unstable potential in the background of a dilaton black hole. A realistic black hole in four dimensions possesses the potential barrier for linear field perturbations. We model this barrier — the greybody factor — for spherically-symmetric perturbations in the toy model by adding a coupling between the scalar field and dilaton. We compute analytically the decay rate for the black hole in thermal equilibrium (Hartle–Hawking state) and for the radiating black hole in empty space (Unruh state). Our results show that, contrary to the Hartle–Hawking vacuum, the decay probability of the Unruh vacuum remains exponentially suppressed at all black hole temperatures. We argue that this result holds also in four dimensions.

*ashkerin@umn.edu

†ssibiryakov@perimeterinstitute.ca

Contents

1 Introduction **1**

2 Setup **4**
2.1 Background geometry 4
2.2 Massive scalar field with a dilaton coupling 5
2.3 Bounce solution and tunneling rate 8
2.4 Tunneling in the inverted Liouville potential 9

3 Decay of the Hartle–Hawking vacuum **12**
3.1 Tunneling in the black hole vicinity 12
3.2 Sphaleron at high temperature: weak and strong barriers 14
3.3 Decay probability 18

4 Decay of the Unruh vacuum **22**
4.1 Tunneling near horizon 22
4.2 Stochastic jumps at high temperature 24

5 Conclusions **27**

A Dilaton black holes **29**

B Schwarzschild black hole in four dimensions **30**
B.1 Mode potential 30
B.2 Hartle–Hawking sphaleron 31

C Linear modes and Green's functions **34**
C.1 Effective potential, modes and scattering coefficients 34
C.2 Green's functions in the asymptotic regions 35
C.3 Calculation of the Green's functions 38

1 Introduction

The problem of catalysis of vacuum decay by black holes [1–4] has recently received significant attention in view of its possible relevance for phenomenology [5–16]. In the Standard Model, the loop-corrected Higgs field potential may develop large negative values at large field values, which makes the low-energy electroweak vacuum metastable [17–23]. Requirement that the lifetime of the vacuum exceeds the age of the Universe puts constraints on the parameters

of the Standard Model, of its possible extensions, and of systems and environments which catalyze vacuum decay, including black holes; see, e.g., [24] for a review.

The catalyzing effect of a black hole (BH) is two-fold. First, it is a local spacetime inhomogeneity. Hence, as many types of impurities, it can facilitate nucleation of bubbles of true vacuum in its vicinity. Second, BHs excite the quantum vacuum producing Hawking radiation. As any field excitation, this radiation is expected to increase the decay rate. For small enough BHs, the catalyzing effects due to curved geometry and quantum excitations may be equally important.

In the semiclassical regime, the vacuum decay is described by a (complex) classical solution of field equations. The solution — bounce — saturates the amplitude of transition from the false to the true vacuum regions. It is important to note that the vacuum is defined not only by classical field expectation values but also by the state of quantum fluctuations around these values. Different false vacuum states reveal themselves through different boundary conditions imposed on the bounce.

It is well-known how to obtain the bounce solution in equilibrium systems [25–28]. One rotates the system to the Euclidean time and looks for a regular solution satisfying appropriate boundary conditions. In the case of BHs, this prescription leads to a periodic Euclidean bounce whose period is inversely proportional to the BH temperature $T_{\rm BH}$, or to a static solution — sphaleron. The solution with the smallest Euclidean action dominates and describes vacuum transitions catalyzed by a BH in the presence of thermal bath of temperature $T_{\rm BH}$. This state of a BH in thermal equilibrium is known as the Hartle–Hawking vacuum [29]. The decay rate of the Hartle–Hawking vacuum is not exponentially suppressed at high temperatures, reflecting the fact that thermal field fluctuations trigger vacuum decay with order-one probability once their average energy exceeds the height of the barrier separating the vacua.

Realistic BHs, however, are not in thermal equilibrium with their environment. In particular, this is true for hypothetical small primordial BHs that could exist in the early Universe but are completely evaporated by now [30–38]. At the late stage of evaporation, a BH radiates at energies comparable to the Planck scale, much above the temperature possibly attained in the primordial plasma. From the perspective of Standard Model vacuum decay, such near-Planckian BHs are of principal interest. This is because the bounce mediating decay of the electroweak vacuum probes field values near the minimum of the Higgs quartic coupling which, for the measured values of the Standard Model parameters [39], approaches the Planck scale.

The above considerations motivate to look for an approach to vacuum decay that can handle such non-equilibrium systems as a hot isolated BH placed in a comparatively low energy environment. This system is described by the Unruh state [40]. In the Unruh vacuum, the BH emits Hawking radiation but does not receive anything from asymptotic infinity. The Euclidean prescription described above is not suitable for a BH in the Unruh vacuum.

It is clear why the decay of the Hartle–Hawking vacuum is unsuppressed at high temperatures. It is much less clear if the Unruh vacuum decay is unsuppressed at high temperatures. From studying vacuum transitions in thermal equilibrium we know that to trigger decay one needs to form a field fluctuation that is coherent on a certain length scale typically associated with the Compton wavelength of the free field. Such fluctuation is represented by the sphaleron. It is not clear what the analog of the sphaleron in the Unruh vacuum is.

In Ref. [41] we have suggested a method to compute the Unruh vacuum decay rate using complex tunneling solutions [42–46].[1] The method accounts for the quantum state of the false vacuum and, hence, it allows one to discriminate between the Hartle–Hawking and Unruh vacua. The key ingredient is the correspondence between the quantum state and the boundary conditions on the bounce. The boundary conditions turn out to be the same as for the time-ordered Green's function in the corresponding vacuum. In the case of Hartle–Hawking vacuum the method reproduces the Euclidean time formalism used in previous works on BH catalysis of vacuum decay [5–8]. The Unruh vacuum provides a genuinely new application of the method. For explicit calculations Ref. [41] adopted a toy two-dimensional model consisting of a real scalar field in the background of a dilaton BH.[2] Thanks to the choice of the tunneling potential, bounce solutions and associated decay rates were found analytically, both for the Hartle–Hawking and Unruh vacua, and both in the BH vicinity and far from it.

In the model of [41], the exponential suppression of the Unruh vacuum decay rate vanishes at high temperatures. We would like to see if this result holds also in a realistic case like the Schwarzschild BH in four dimensions. The model of [41] lacks two important features of the realistic setup. First, a field in Schwarzschild background feels a centrifugal barrier whose height is inversely proportional to the square of the BH size and, hence, grows with the BH temperature. There is no such barrier in two dimensions. Its presence in four dimensions may significantly affect the Unruh vacuum decay rate at high temperatures [11]. Second, the flux of Hawking quanta in four dimensions spreads inversely proportional to the area of the sphere encompassing the BH at a given distance. This reduces the density of Hawking radiation away from the BH and is expected to further suppress the tunneling rate of Unruh vacuum [11, 52].

The present paper is a follow-up of Ref. [41]. Its goal is to compute the rate of decay of the Unruh vacuum in a model containing the temperature-dependent barrier for massive scalar modes. This will bring us one step closer to the problem of vacuum decay in the realistic BH background in four dimensions. To emulate the barrier, we modify the model of [41] by adding a coupling between the tunneling scalar field and the dilaton. Note that the area growth in four dimensions remains unaccounted for in our setup. We will discuss

[1] See [47–51] for related approaches to tunneling.

[2] The back-reaction of the tunneling field on spacetime geometry is taken to be negligible in [41].

qualitatively its possible effect on vacuum decay at the end of the paper.

The scalar-dilaton coupling constant that controls the strength of the barrier is a free parameter of the model. When it is zero, the model reduces to the one studied in [41]. In particular, the exponential suppression of the Unruh vacuum goes to zero at high BH temperatures. The main result of this paper is that, whenever the coupling is non-zero, the decay of the Unruh vacuum remains exponentially suppressed at all temperatures.[3]

The paper is organized as follows. In sec. 2 we recapitulate the results of [41], and describe the toy model used to study vacuum decay. We outline the technique to find the tunneling solution and illustrate it in the case of vacuum decay in flat space. In sec. 3 we study the decay of the Hartle–Hawking vacuum in the BH vicinity. The results of this study are important in two respects. First, it is instructive to compare transitions from the Hartle–Hawking vacuum to those from the Unruh vacuum, since the difference between the two states is entirely due to the different population of Hawking quanta, i.e., due to the different quantum vacuum structure. Second, and more importantly, the Hartle–Hawking vacuum decay can be straightforwardly studied in four dimensions. Hence, we can directly compare the physics of tunneling in our toy model for the different values of the scalar-dilaton coupling and in a four-dimensional scalar field theory in the Schwarzschild background. We can then select the values of the coupling parameter for which we see the best agreement in the behavior of the two systems.

In sec. 4 we study the decay of the Unruh vacuum. We analytically construct the Unruh bounces for the range of the scalar-dilaton couplings emulating the four-dimensional behavior and compute the associated decay rates. Not all values of BH temperature admit analytic bounce solution. When no such solution is available, we employ a stochastic estimate of the decay rate. We find that the exponential suppression of the Unruh vacuum decay rate is constant in the high temperature limit.

We conclude in sec. 5. The main text is accompanied by several appendices.

2 Setup

2.1 Background geometry

We consider a real scalar field in the background of a dilaton BH in two dimensions [53]. The dilaton BH is characterized by the temperature $T_{\rm BH}$ and mass M which are a priori

[3] More precisely, the lower bound on the coupling comes from the requirement for the tunneling action to be large at all $T_{\rm BH}$. We will see that the bound is proportional to another coupling constant that controls the semiclassical expansion and can be made arbitrarily small.

independent of each other.[4] The BH background is set up by the metric $g_{\mu\nu}$ and the dilaton field ϕ. As discussed in [41], the only region that is relevant for vacuum decay is the patch of the BH spacetime outside the horizon. It is convenient to introduce tortoise coordinates (t, x) covering this patch. Then the metric is read off from the line element

$$\mathrm{d}s^2 = \Omega(x)(-\mathrm{d}t^2 + \mathrm{d}x^2) \,, \tag{2.1}$$

where the conformal factor takes the form

$$\Omega(x) = \frac{1}{1 + \mathrm{e}^{-2\lambda x}} \,. \tag{2.2}$$

The parameter λ is related to the BH temperature as $\lambda = 2\pi T_{\rm BH}$. For the sake of brevity, we will refer to λ itself as temperature. The horizon is located at $x \to -\infty$. Near horizon, the conformal factor behaves as $\Omega(x) \approx \mathrm{e}^{2\lambda x}$. Substituting this to eq. (2.1), we obtain the two-dimensional Rindler metric. Thus, the near-horizon region is approximated by the Rindler spacetime. The physical size of this region is

$$l_h \sim \int_{-\infty}^{0} \mathrm{d}x\sqrt{\Omega} \sim \frac{1}{\lambda} \,. \tag{2.3}$$

In the opposite limit, $x \to \infty$, the metric is asymptotically flat. Finally, the dilaton profile is given by

$$\phi = -\frac{1}{2}\ln\left[\frac{M}{2\lambda}\left(1 + \mathrm{e}^{2\lambda x}\right)\right] \,. \tag{2.4}$$

In appendix A we discuss dilaton BHs in more details. The vacuum boundary conditions are imposed in the remote past, $t \to -\infty$, on both sides of the physical patch, $x \to \pm\infty$.

2.2 Massive scalar field with a dilaton coupling

To study tunneling in the BH background, we consider the following scalar field theory

$$S = \frac{1}{\mathrm{g}^2}\int \mathrm{d}^2x\sqrt{-g}\left(-\frac{1}{2}g^{\mu\nu}\partial_\mu\varphi\partial_\nu\varphi - \frac{m^2\varphi^2}{2} - Q\mathrm{e}^{2\phi}\varphi^2 - V_{\rm int}(\varphi)\right) \,. \tag{2.5}$$

Here $V_{\rm int}(\varphi)$ is the interaction part of the tunneling potential to be specified below. So far it suffices to assume that the false vacuum is located at $\varphi = 0$ where the potential vanishes, $V_{\rm int}(0) = 0$. Next, $Q > 0$ is the nonminimal coupling (of mass dimension 2) of the scalar field

[4] This is different from the four-dimensional Schwarzschild case where $T_{\rm BH}$ and M are related by

$$T_{\rm BH} = \frac{M_{\rm Pl}^2}{8\pi M}$$

with $M_{\rm Pl}$ the Planck mass.

to the dilaton. We will see shortly that this coupling gives rise to the temperature-dependent barrier in the potential for linearized field perturbations, which is similar to the centrifugal barrier in the four-dimensional Schwarzschild spacetime. We will refer to it as "dilaton barrier" in what follows. The small coupling constant $\mathrm{g} \ll 1$ controls the semiclassical expansion in the model.

In the background specified by eqs. (2.1), (2.2) and (2.4), the action (2.5) becomes

$$S = \frac{1}{\mathrm{g}^2}\int \mathrm{d}t\mathrm{d}x \left(-\frac{1}{2}\eta^{\mu\nu}\partial_\mu\varphi\partial_\nu\varphi - \frac{1}{2}\Omega m^2\varphi^2 - \frac{Q\Omega'}{M}\varphi^2 - \Omega V_{\rm int}(\varphi)\right) , \tag{2.6}$$

where $\eta^{\mu\nu} = \mathrm{diag}(-1,1)$ is the Minkowski metric. We see that the dependence on the background is contained entirely in the (position-dependent) potential of the field φ.

Let us study linear perturbations around the false vacuum $\varphi = 0$. To this end, we neglect the self-interaction part of the potential $V_{\rm int}$, and decompose φ using a complete set of positive- and negative-frequency modes:

$$\varphi^+_\omega(t,x) = f_\omega(x)\mathrm{e}^{-i\omega t} , \quad \varphi^-_\omega(t,x) = f^*_\omega(x)\mathrm{e}^{i\omega t} , \quad \omega > 0 . \tag{2.7}$$

The equation for f_ω follows from the linearized field equation for φ and reads

$$-f''_\omega + U_{\rm eff}(x) f_\omega = \omega^2 f_\omega , \tag{2.8}$$

where prime denotes derivative with respect to x. This is the Schrödinger equation with the potential

$$U_{\rm eff}(x) = m^2\Omega + \frac{2Q}{M}\Omega' . \tag{2.9}$$

It is instructive to compare it with the analogous potential for spherically-symmetric linear perturbations of the massive scalar field in the four-dimensional Schwarzschild background, which we review in appendix B.1. The latter admits similar form as in eq. (2.9) (with a different Ω), with the factor in front of Ω' being proportional to the BH temperature. To reproduce this behavior, in what follows we take the mass of the dilaton BH to be temperature-dependent,

$$M(\lambda) = \frac{M_0^2}{\lambda} , \tag{2.10}$$

where M_0 is a constant of mass dimension 1.[5] In other words, we enforce the relation between the BH mass and temperature as in General Relativity. Using eq. (2.2), we obtain

$$U_{\rm eff}(x) = \frac{m^2}{1+\mathrm{e}^{-2\lambda x}} + \frac{2q\lambda^2\mathrm{e}^{-2\lambda x}}{(1+\mathrm{e}^{-2\lambda x})^2} , \tag{2.11}$$

where we introduced $q = 2Q/M_0^2$. The first term in this expression describes a smooth interpolation between the near-horizon and asymptotically-flat regions, while the second term generates a barrier separating these regions, see Fig. 1.

[5]The constant M_0 is subject to certain conditions ensuring that the back-reaction of vacuum decay on the background geometry is negligible; see appendix A. Apart from this, it is arbitrary.

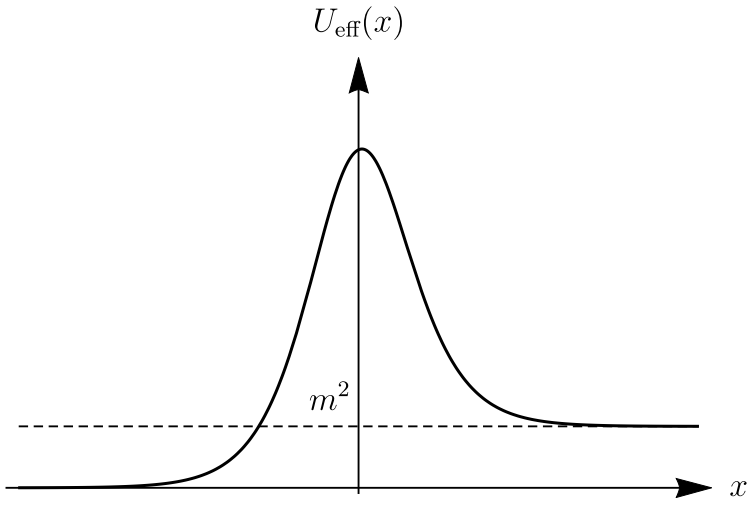


Figure 1: Potential for massive linear scalar modes in the two-dimensional dilaton BH background in the presence of the scalar-dilaton coupling with $q > m^2/(2\lambda^2)$. The horizon is located at $x \to -\infty$.

Two comments are in order regarding the form of the potential (2.11). First, at $2q\lambda^2 > m^2$, the height of the barrier exceeds m^2, and the maximum of the potential is achieved near $x = 0$, see Fig. 1. This is expected to significantly affect the properties of the tunneling solution in the vicinity of the BH. Second, the mode equation (2.8) with the potential (2.11) admits a general solution in terms of the hypergeometric function. This means, in particular, that the Green's functions of φ can be found analytically both near and far from the horizon. Thus, the linear part of the theory (2.5) retains all good features of the model without the scalar-dilaton coupling that was studied in [41]. Further properties of the potential (2.11) are discussed in appendix C.

To match the greybody factor of the four-dimensional Schwarzschild geometry, the parameter q in eq. (2.11) must be of the order of one; see appendix B.1. However, our goal is not to match exactly the two-dimensional model with a spherical reduction of some four-dimensional theory. Such a matching would anyway be imperfect due to the difference in Ω. Instead, we aim at identifying essential features of vacuum decay in four dimensions and modeling them in the two-dimensional setup. As we believe that the presence of barrier is important, we expect that the qualitative agreement between the physics of tunneling in the two and four dimensions is achieved once q exceeds $m^2/(2\lambda^2)$, which at high temperature can be much less than one. We will see in secs. 3 and 4 that it suffices to study the case

$$m^2/(2\lambda^2) \lesssim q \ll 1 \,. \tag{2.12}$$

This limit significantly simplifies the calculation of the Green's functions which is performed in appendix C.

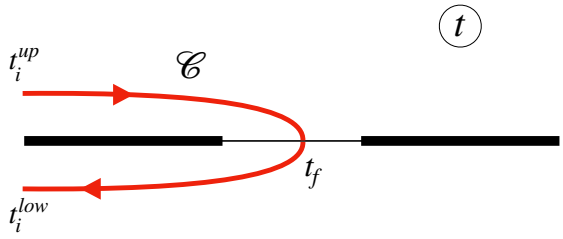


Figure 2: Contour $\mathscr{C}$ in the complex time plane for the calculation of the vacuum decay probability. We show the case when the branch-cuts of the bounce (shown with thick black lines) lie on the real axis. This corresponds to a theory with the scalar potential unbounded from below.

2.3 Bounce solution and tunneling rate

Here we summarize the results of Ref. [41] concerning the construction of bounce solutions. Bounce $\varphi_{\rm b}$ is a regular solution of the field equations that saturates the transition amplitude from the false vacuum initial state to the basin of attraction of true vacuum. In our case, the field equation of motion is

$$\Box\varphi - U_{\rm eff}(x)\varphi - \Omega V'_{\rm int}(\varphi) = 0 \,. \tag{2.13}$$

The bounce lives on a contour $\mathscr{C}$ in the complex time plane shown in Fig. 2. The contour runs from the initial moment of time in the asymptotic past, $t = t_i^{up}$ shifted to the upper half plane, to the final moment $t = t_f$ and back to the asymptotic past, $t = t_i^{low}$ in the lower half plane. The contour must bypass the singularities of the bounce. Assuming that the bounce is unique, its values on the upper and lower sides of the contour are complex conjugated, hence at $t = t_f$ it is real and can be analytically continued along the real time axis where it describes the evolution of the field after tunneling.

In the limits $t \to t_i^{up}$ and $t \to t_i^{low}$ the bounce must satisfy boundary conditions imposed by the false vacuum state. These boundary conditions turn out to be the same as for the time-ordered Green's function in the corresponding vacuum X [41]. The latter is defined as a time-ordered average of the linear field operators $\hat\varphi$ in the state X,

$$\mathcal{G}_X(t,x;t',x') = {}_X\langle T(\hat\varphi(t,x)\hat\varphi(t',x'))\rangle_X \,. \tag{2.14}$$

In turn, the field operator is constructed out of the complete set of modes (2.7) in the standard way [54]. Explicit expressions for the time-ordered Green's functions in the Hartle–Hawking and Unruh vacua are presented in appendix C.

A Green's function satisfies the equation

$$(\Box - U_{\rm eff}(x))\,\mathcal{G}_X(t,x;t',x') = i\delta(t-t')\delta(x-x') \,. \tag{2.15}$$

Using this property, the field equation (2.13) can be recast into the integral form. To select a particular solution—bounce—of the integral equation, one should, first, adopt the time-integration contour $\mathscr{C}$ in the complex time plane and, second, choose the Green's function corresponding to a particular false vacuum X. Thus, we arrive at

$$\varphi_{\rm b}(t,x) = -i\int_{\mathscr{C}} {\rm d}t' \int_{-\infty}^{\infty} {\rm d}x'\, \mathcal{G}_X(t,x;t',x')\Omega(x')V'_{\rm int}(\varphi_{\rm b}(t',x'))\ . \tag{2.16}$$

This form of the bounce equation will be useful in what follows.

Finally, let us discuss the tunneling rate Γ. The latter is defined as the probability of tunneling per unit time. We are interested in the main exponential dependence and write

$$\Gamma \sim {\rm e}^{-B}\ . \tag{2.17}$$

The coefficient B is the sum of the imaginary part of the bounce action computed along the contour $\mathscr{C}$ and a boundary term representing the initial-state contribution. One can show that the boundary term cancels upon integration by parts in the action and one is left with [41]

$$B = -\frac{i}{{\rm g}^2}\int_{\mathscr{C}} {\rm d}t \int_{-\infty}^{\infty} {\rm d}x \left(\frac{1}{2}\varphi_{\rm b}V'_{\rm int}(\varphi_{\rm b}) - V_{\rm int}(\varphi_{\rm b})\right)\ . \tag{2.18}$$

2.4 Tunneling in the inverted Liouville potential

In general, solving eq. (2.16) (or eq. (2.13) on the contour $\mathscr{C}$ with the vacuum boundary conditions) requires a numerical procedure. A big simplification of the problem happens in theories where the nonlinear core of the bounce, where it probes the true vacuum region, is much smaller in size than the Compton wavelength of the free field $\propto m^{-1}$. Then the source in the integral (2.16) is essentially point-like, and the solution outside the core is simply proportional to the Green's function $\mathcal{G}_X$. On the other hand, the core itself can be found by neglecting the mass term in the field equation (2.13). The full solution is constructed by matching the long-distance asymptotics of the core with the short-distance asymptotics of the Green's function.

In [41], the interaction potential $V_{\rm int}$ has been studied for which the above procedure of finding the bounce solution works and yields analytic result. This is the negative Liouville potential,

$$V_{\rm int}(\varphi) = -2\kappa\left({\rm e}^{\varphi} - 1\right) \tag{2.19}$$

with $\kappa > 0$. In flat spacetime, the full scalar field potential $V(\varphi) = \frac{1}{2}m^2\varphi^2 + V_{\rm int}(\varphi)$ is shown in Fig. 3. To ensure the applicability of the split-and-match procedure, the following relation between the parameters is adopted

$$\ln\frac{m}{\sqrt{\kappa}} \gg 1\ . \tag{2.20}$$

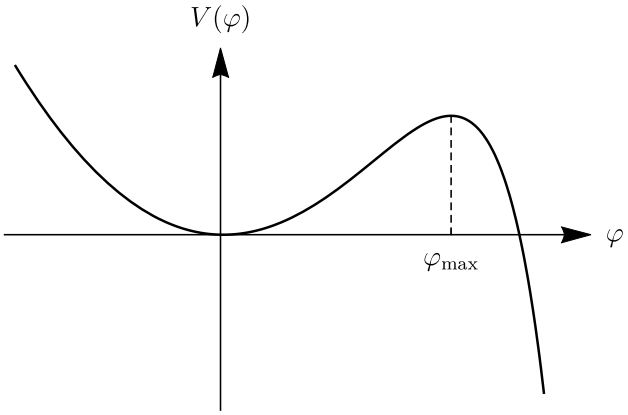


Figure 3: The scalar field potential.

Thanks to this hierarchy, the theory possesses two intrinsic energy scales: the mass scale m and the scale associated with the maximum of the scalar potential separating the false and true vacua $m \ln \frac{m}{\sqrt{\kappa}}$. Generally speaking, the first controls the width of the linear tail of the bounce, while the second determines the size of its core. The maximum of the potential is located at

$$\varphi_{\max} \approx 2 \ln \frac{m}{\sqrt{\kappa}} \,, \tag{2.21}$$

where we have reatined only the leading logarithmic term.

To illustrate the matching procedure outlined above, let us discuss bounce in the flat-space Minkowski vacuum (see Ref. [41]). Assume that the only singularities of the bounce are located on the real-time axis. Then, the contour $\mathscr{C}$ can be deformed into the contour $\mathscr{C}'$ that runs along the Euclidean time axis, see Fig. 4. The vacuum boundary condition at $\mathscr{C}$, which is provided by the Feynman Green's function, becomes the vanishing boundary condition at $\mathscr{C}'$. Hence, the standard Euclidean approach is reproduced [25, 26].

To find the core of the bounce, we neglect the mass term in eq. (2.13) and, using eq. (2.19), obtain

$$\Box \, \varphi_{\rm b}\big|_{\rm core} + 2\kappa \mathrm{e}^{\varphi_{\rm b}|_{\rm core}} = 0 \,. \tag{2.22}$$

This is the Liouville equation, and its general solution is known. Next, the linear tail of the bounce is proportional to the Feynman Green's function

$$\mathcal{G}_F(-i\tau, x; 0, 0) = \frac{1}{2\pi} K_0 \left(m\sqrt{\tau^2 + x^2 + i\epsilon} \right) \,, \tag{2.23}$$

where $\tau = it$ is the Euclidean time coordinate. The core and the tail are matched in the region where, on the one hand, the solution to the Liouville equation is linearized and, on the other hand, the Green's function is approximated by its short-distance asymptotics. We

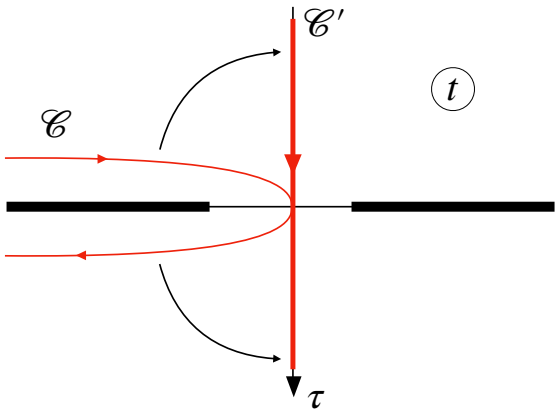


Figure 4: Deformation of the contour $\mathscr{C}$ into the Euclidean time contour $\mathscr{C}'$ used for the calculation of the flat-space Minkowski bounce. Black lines denote singularities of the bounce.

obtain[6]

$$\varphi_{\rm b}|_{\rm core} = \ln\left[\frac{4C_M^2}{(1+\kappa C_M^2(\tau^2+x^2))^2}\right] \tag{2.24a}$$

$$\varphi_{\rm b}|_{\rm tail} = 8\pi\mathcal{G}_F(-i\tau, x; 0, 0)\ , \tag{2.24b}$$

where $C_M = m^2 {\rm e}^{2\gamma_E}/(2\kappa)$. The matching region is defined by

$$(C_M\sqrt{\kappa})^{-1} \ll \sqrt{\tau^2+x^2} \ll m^{-1}\ .$$

Its existence is ensured by eq. (2.20). We see that the bounce is real for real τ, vanishes at infinity and has zero time derivative at $\tau = 0$. Hence, it is a valid tunneling solution. Moreover, it has no singularities apart from the ones on the real-time axis, which justifies the deformation of the contour $\mathscr{C}$ into $\mathscr{C}'$.

The tunneling suppression is given by eq. (2.18) where one should substitute the core of the bounce (2.24a). We obtain[7]

$$B_M = \frac{16\pi}{{\rm g}^2}\left(\ln\frac{m}{\sqrt{\kappa}} + \gamma_E - 1\right)\ , \tag{2.25}$$

where γ_E is the Euler constant. We observe that the suppression is enhanced by the large logarithm (2.20).

[6]Solving the partial differential equation for the core (2.22) becomes trivial once one takes into account that the solution providing the dominant decay channel is spherically-symmetric [55–57]. Note, however, that eq. (2.24a) can be derived without adopting spherical symmetry from the onset; in fact, the latter follows from the form of the Feynman Green's function (2.23).

[7]The corrections to eq. (2.25) are of order ${\rm g}^{-2} \times o(1)$.

In the BH background (2.2), the linearized field equation (2.8) is still exactly solvable, and this allows us to compute explicitly the Green's functions of interest. The solvability of the equation for the core of the bounce is lost, but can be recovered in the two regions: near the horizon where the metric is approximately Rindler, and far away from the BH where the spacetime is asymptotically flat. From eqs. (2.2) and (2.11) we see that the two regions are defined by $x < 0$, $|x| \gg \lambda^{-1}$ and $x > 0$, $|x| \gg \lambda^{-1}$, respectively. Although we do not have the explicit bounce solution in the transition region $|x| \lesssim \lambda^{-1}$, we will still be able to draw a qualitative picture of the evolution of the bounce across this region.

3 Decay of the Hartle–Hawking vacuum

Here we study transitions from the Hartle–Hawking state in the model defined by eqs. (2.2), (2.6) and (2.19). This state corresponds to the BH in thermal equilibrium, for which our method reduces to the standard Euclidean time approach. It provides a benchmark for later study of transitions from the Unruh vacuum. Besides, the relevant configuration describing vacuum decay from the state in thermal equilibrium is readily found in the four-dimensional BH background. Comparing the results in two and four dimensions, we will identify the regime in which our model adequately mimics catalysis of false vacuum decay by the four-dimensional Schwarzschild BH. In this and the following sections we will assume $\lambda \gg m$, which allows us to treat the problem analytically.

3.1 Tunneling in the black hole vicinity

Consider first the near-horizon region where the BH geometry is approximated by the Rindler spacetime. The bounce solution is found by applying the split-and-match procedure described in sec. 2.4. It lives on the contour $\mathscr{C}$ stretched along the real-time axis. The contour can be deformed partially to the Euclidean time domain as shown in Fig. 5. Then the thermal boundary condition in the asymptotic past imposed at $\mathscr{C}$ transforms into the periodic boundary condition imposed at the Euclidean segment $-\pi/\lambda < \tau < \pi/\lambda$ of $\mathscr{C}'$ (where $\tau = it$ denotes the Euclidean time coordinate) [41]. This way one recovers the standard Euclidean prescription for the thermal bounce [58–60].

The equation for the nonlinear core of the Hartle–Hawking bounce takes the form (cf. eq. (2.22))

$$\Box\, \varphi_{\rm b}\big|_{\rm core} + 2\kappa \mathrm{e}^{2\lambda x + \varphi_{\rm b}|_{\rm core}} = 0\,, \tag{3.1}$$

where we assumed that the core fits the near-horizon region. This equation admits analytic general solution. On the other hand, the linear tail of the bounce is proportional to the time-ordered Hartle–Hawking Green's function $\mathcal{G}_{HH}$ computed in the BH vicinity. Overall,

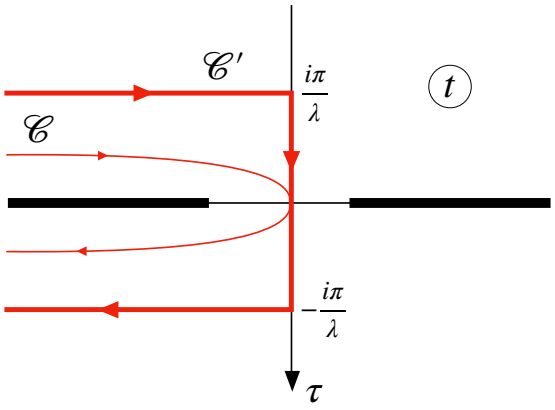


Figure 5: Deformation of the contour $\mathscr{C}$ into $\mathscr{C}'$ containing the Euclidean time segment which is used for the calculation of the Hartle–Hawking bounce.

we obtain [41]

$$\varphi_{\rm b}|_{\rm core} = \ln\left[\frac{\lambda^2 b_{HH}}{\kappa\left(\operatorname{ch}\lambda(x-x_{HH}) - \sqrt{1-b_{HH}}\cos\lambda\tau\right)^2}\right] - 2\lambda x \tag{3.2a}$$

$$\varphi_{\rm b}|_{\rm tail} = 8\pi\mathcal{G}_{HH}(-i\tau, x; 0, x_{HH}) \tag{3.2b}$$

Here the parameter b_{HH} is determined from matching the core with the tail, and $x_{HH} < 0$ is the position of the center of the bounce.

Let us see how the core and the tail of the bounce match each other. This is readily done if $b_{HH} \ll 1$, since in this case the matching region exists in the Euclidean strip of the contour $\mathscr{C}'$. In the matching region, on the one hand, the core of the bounce linearizes, that is, the first term in the denominator of $\varphi_{\rm b}|_{\rm core}$ dominates over the second one, and, on the other hand, the tail of the bounce is taken in the limit $|x - x_{HH}| \ll m^{-1}$. The expression for $\mathcal{G}_{HH}$ in this limit is given in eq. (C.11). One obtains the following relation between the parameters

$$b_{HH} = \frac{\kappa}{4\lambda^2}\mathrm{e}^{\frac{4\lambda}{m+q\lambda}-2\lambda x_{HH}}\ . \tag{3.3}$$

By extending the matching region to the parts of the contour going parallel to the real-time axis, one can show that eq. (3.3) remains valid as long as $b_{HH} \leq 1$ [41]. On the other hand, no matching is possible if $b_{HH} > 1$.

We see that the Hartle–Hawking bounce is characterized by one free parameter x_{HH}, the position of the center of the bounce. Existence of one-parameter family of solutions is a consequence of the (approximate) Rindler symmetry of the BH vicinity. The flat direction corresponding to x_{HH} is tilted by the terms in the BH metric that discriminate it from the Rindler metric. Hence, one expects to get a unique tunneling solution with the least

suppression. The most likely candidate for such a solution is a static sphaleron [61] (see also [3, 5]). It is obtained in the limit $b_{HH} = 1$ which is achieved when x_{HH} takes the value

$$x_{HH,\mathrm{sph}} = \frac{2}{m + q\lambda} - \frac{1}{\lambda} \ln \frac{2\lambda}{\sqrt{\kappa}} \,. \tag{3.4}$$

The core of the sphaleron is given by

$$\varphi_{\mathrm{sph}}\big|_{\mathrm{core}} = \ln \left[\frac{\lambda^2}{\kappa \,\mathrm{ch}^2 \left(\lambda(x - x_{HH,\mathrm{sph}})\right)} \right] - 2\lambda x \,. \tag{3.5}$$

Note that, strictly speaking, the static sphaleron does not satisfy the vacuum boundary conditions imposed at $\mathscr{C}$. Nevertheless, as explained in [41], it appears as the end-point configuration of valid tunneling solutions and correctly describes the tunneling rate. Having this in mind, in the rest of this section we will focus on the sphaleron solution.

At low and moderate temperature, the coordinate of the sphaleron's center is negative, $x_{HH,\mathrm{sph}} < 0$, so it is comfortably inside the near-horizon region. In the case without the dilaton barrier, $q = 0$, the center of the sphaleron shifts to the right as the temperature increases and at $\lambda_{HH,0} \simeq \frac{m}{2} \ln \frac{m}{\sqrt{\kappa}}$ it reaches $x = 0$. At this point the sphaleron does not fit into the near-horizon region anymore and sticks out into the flat space at $x > 0$ [41]. Our goal now is to understand what happens with the sphaleron at $\lambda \sim \lambda_{HH,0}$ in the presence of the barrier.

3.2 Sphaleron at high temperature: weak and strong barriers

For static configurations, the equation of motion (2.13) reduces to the ordinary differential equation

$$\varphi''_{\mathrm{sph}} - (m^2\Omega + q\lambda\Omega')\varphi_{\mathrm{sph}} + 2\kappa\Omega\, \mathrm{e}^{\varphi_{\mathrm{sph}}} = 0 \,, \tag{3.6}$$

which is straightforward to solve numerically. It is instructive, however, to consider a simplified version of eq. (3.6) which can be studied analytically. To this purpose, we replace the function $\Omega(x)$ in the brackets by the Heaviside θ-function and its derivative by the δ-function. Physically, this means that we are neglecting the width of the dilaton barrier compared to the size of the sphaleron. This is certainly a good approximation for the sphaleron tails which have width of order m^{-1}. On the other hand, the sphaleron core has width $\sim \lambda^{-1}$ which is comparable to the width of the barrier. Below we will encounter configurations with the core of the sphaleron in the immediate neighborhood of the barrier. For these configurations we do not expect an exact quantitative agreement with the solution of the original eq. (3.6). Nevertheless, we will see that they capture the right qualitative behavior.

We also simplify the last — Liouville — term in eq. (3.6). We cannot simply set Ω to the θ-function in it as this would lead to the loss of sphaleron solutions in the near-horizon

region. Instead, we approximate Ω with a pure exponential $\mathrm{e}^{2\lambda x}$ at $x<0$ and 1 at $x>0$. In other words, we assume that the metric is exactly Rindler to the left from the barrier and flat to the right of it. Overall, the approximate equation we will analyze has the following form,

$$\varphi''_{\rm sph} - \big(m^2\theta(x) + q\lambda\delta(x)\big)\varphi_{\rm sph} + 2\kappa\big(\theta(-x)\mathrm{e}^{2\lambda x} + \theta(x)\big)\mathrm{e}^{\varphi_{\rm sph}} = 0\,. \tag{3.7}$$

It is straightforward to solve this equation to the left and to the right of the barrier. The solutions bounded at $x\to\pm\infty$ are:

$$\varphi_{\rm sph}\Big|_{\rm left} = \ln\left[\frac{\lambda^2}{\kappa\,\mathrm{ch}^2(\lambda(x-x_{\rm sph,L}))}\right] - 2\lambda x\,, \tag{3.8}$$

$$\varphi_{\rm sph}\Big|_{\rm right} = \begin{cases} \ln\left[\frac{\lambda_0^2}{\kappa\,\mathrm{ch}^2(\lambda_0(x-x_{\rm sph,R}))}\right]\,, & \text{core} \\ \frac{2\lambda_0}{m}\mathrm{e}^{-m|x-x_{\rm sph,R}|}\,, & \text{tail} \end{cases} \tag{3.9}$$

where λ_0 satisfies

$$\frac{\lambda_0}{\ln(2\lambda_0/\sqrt{\kappa})} = m \quad\Rightarrow\quad \lambda_0 \simeq m\ln\frac{m}{\sqrt{\kappa}}\,. \tag{3.10}$$

At $x=0$ the two solutions (3.8), (3.9) must be matched continuously, whereas the derivative must have a jump due to the δ-function in the equation,

$$\varphi_{\rm sph}(0)\Big|_{\rm right} = \varphi_{\rm sph}(0)\Big|_{\rm left} \equiv \varphi_{\rm sph}(0)\,, \tag{3.11a}$$

$$\varphi'_{\rm sph}(0)\Big|_{\rm right} = \varphi'_{\rm sph}(0)\Big|_{\rm left} + q\lambda\varphi_{\rm sph}(0)\,. \tag{3.11b}$$

Let us assume first that the solution on the right is given purely by the tail, i.e., the core of the sphaleron lies deep in the near-horizon region. Then the matching conditions (3.11) lead to the equation on $x_{\rm sph,L}$,

$$1 - \mathrm{th}(\lambda x_{\rm sph,L}) = \frac{m+q\lambda}{2\lambda}\ln\left[\frac{\lambda^2}{\kappa\,\mathrm{ch}^2(\lambda x_{\rm sph,L})}\right]\,. \tag{3.12}$$

To proceed, it is convenient to parameterize q as

$$q = \frac{a}{\ln(m/\sqrt{\kappa})}\,. \tag{3.13}$$

For $a>1$, eq. (3.12) has a negative solution for arbitrary value of $\lambda\gg m$, implying that the sphaleron core is always confined to the near-horizon region. This behavior is dramatically different from the case without barrier ($a=0$) and we will call barriers with $a>1$ "strong". Notice that even for a strong barrier q itself can be much smaller than 1.

If $a < 1$, the negative solution to eq. (3.12) grows with temperature and reaches zero at $\lambda \simeq \frac{m}{1-a} \ln \frac{m}{\sqrt{\kappa}}$. The sphaleron stops fitting the near-horizon region and escapes outside. We will refer to this case as "weak barrier". When $x_{\rm sph,L}$ gets close to zero, eq. (3.12) becomes inaccurate because the solution on the right can no longer be approximated by a pure tail. Instead, the sphaleron core is now sitting right on the barrier and we should use the upper expression in eq. (3.9). Let us introduce

$$s_{\rm L} = \lambda \, {\rm th}(\lambda x_{\rm sph,L}) \ , \qquad s_{\rm R} = \lambda_0 \, {\rm th}(\lambda_0 x_{\rm sph,R}) \ . \tag{3.14}$$

Note that we do not require $x_{\rm sph,R}$ ($x_{\rm sph,L}$) to be positive (negative) — these are just the parameters of the solution and can have either sign. The matching conditions (3.11) take the form

$$\lambda^2 - s_{\rm L}^2 = \lambda_0^2 - s_{\rm R}^2 \ , \tag{3.15a}$$

$$s_{\rm L} - s_{\rm R} = \lambda(1-a) \ , \tag{3.15b}$$

where in the second line we substituted eq. (3.13) and neglected terms suppressed by the large logarithm (2.20). The solution reads

$$s_{\rm L} = \frac{\lambda^2(2-2a+a^2) - \lambda_0^2}{2\lambda(1-a)} \ , \qquad s_{\rm R} = \frac{\lambda^2 a(2-a) - \lambda_0^2}{2\lambda(1-a)} \ . \tag{3.16}$$

The conditions $-1 < s_{\rm L}/\lambda, s_{\rm R}/\lambda_0 < 1$ following from the definition (3.14) are satisfied for BH temperatures in the interval

$$\frac{\lambda_0}{2-a} < \lambda < \frac{\lambda_0}{a} \ , \tag{3.17}$$

which is non-empty only for $a < 1$. At the lower end of this interval both $x_{\rm sph,L}$ and $x_{\rm sph,R}$ formally go to $-\infty$, which means that the solution matches to the sphalerons deep in the near-horizon region studied above (the run-away is regularized by replacing the sphaleron core on the right by the tail).

The behavior at the upper end is qualitatively different for the case without barrier ($a = 0$) and with barrier, no matter how weak. In the former case $x_{\rm sph,R} \to 0$ at $\lambda \to \infty$ implying that the field at $x > 0$ represents half of the flat-space sphaleron. At the same time $x_{\rm sph,L} \to +\infty$, which means that the field at $x < 0$ is simply constant. Thus, the two-dimensional BH "cuts the sphaleron in half" [41]. Accordingly, the sphaleron energy is half of that in flat space.

On the other hand, for $a > 0$ both $x_{\rm sph,R}$ and $x_{\rm sph,L}$ run away to $+\infty$ at $\lambda \to \lambda_0/a$. This means that the sphaleron core gets detached from the barrier and shifts into the flat region to the right. At $\lambda > \lambda_0/a$ there are no sphalerons at finite distance from the barrier. Of course, there are still flat-space sphalerons in the asymptotic region $x \to +\infty$ given by

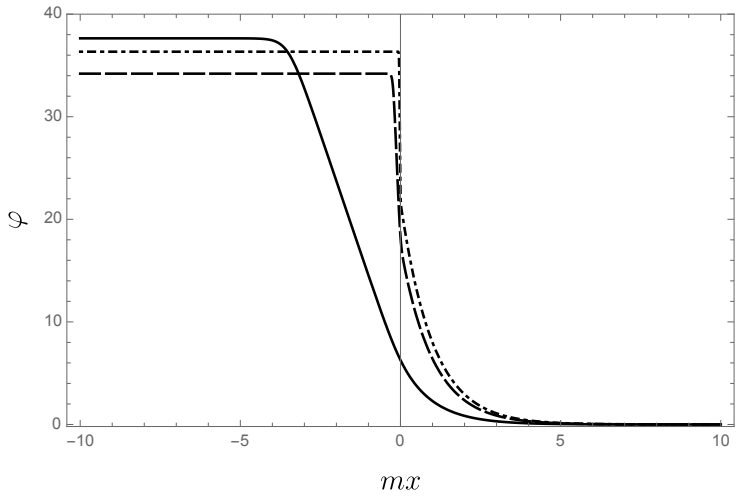


Figure 6: Profiles of the sphaleron in the metric of two-dimensional dilaton BH with strong dilaton barrier. We take $\kappa = 10^{-8}m^2$ and $q = 1.5/\ln\frac{m}{\sqrt{\kappa}}$. Different curves correspond to the following BH temperatures: $\lambda/\left(m\ln\frac{m}{\sqrt{\kappa}}\right) = 0.25$ (solid), 2 (dashed), 10 (dot-dashed).

eq. (3.9) and the Hartle–Hawking vacuum decay proceeds via jumps over these sphalerons in the thermal bath far away from the BH.

The above analysis is confirmed by the direct numerical solution of eq. (3.6). In Figs. 6 and 7 we plot the sphaleron profiles for several values of BH temperature for strong ($a = 1.5$) and weak ($a = 0.5$) barriers. We see that for the strong barrier the sphaleron gets confined to the near-horizon region at all temperatures. By contrast, in the weak barrier case, as the BH temperature increases, the sphaleron shifts from the near-horizon region to be centered on the barrier and then moves further out to the asymptotically flat region.

Which of the two regimes—the weak barrier or the strong barrier—corresponds better to a realistic four-dimensional theory? To answer this question, in appendix B.2 we perform a numerical investigation of the decay of the Hartle–Hawking vacuum in the Schwarzschild background in four dimensions. We focus again on the sphaleron solution since one can argue that it is the most relevant configuration at all BH temperatures [61]. We take the theory of a massive scalar field with a negative quartic self-interaction, which is a prototypical model of the Higgs field and its (loop-corrected) potential. Our analysis shows that the high-temperature Hartle–Hawking sphaleron tends asymptotically to its flat-space counterpart. This means that there are no solutions localized in the near-horizon region of a small Schwarzschild BH in thermal equilibrium. We conclude that the case of weak barrier describes more adequately the physics of vacuum decay in four dimensions. Since our goal is to model the four-dimensional physics as closely as possible, we focus on the weak barrier case $0 < a < 1$ in the rest of the paper.

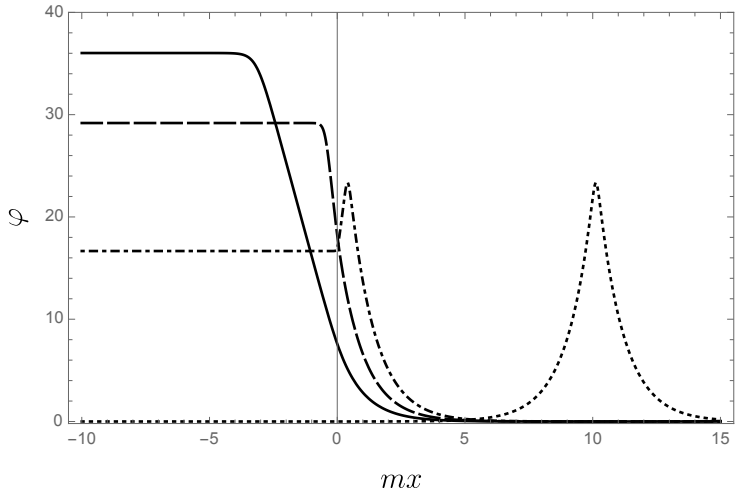


Figure 7: Same as Fig. 6, but now for the case of weak dilaton barrier. We take $\kappa = 10^{-8}m^2$ and $q = 0.5/\ln\frac{m}{\sqrt{\kappa}}$. The BH temperatures are: $\lambda/\left(m\ln\frac{m}{\sqrt{\kappa}}\right) = 0.25$ (solid), 0.66 (dashed), 1.942 (dot-dashed), 1.944 (dotted).

Let us comment on the value of the scalar-dilaton coupling, $q = (\ln\frac{m}{\sqrt{\kappa}})^{-1} \ll 1$, separating the regimes of weak and strong barrier. That in our model this value is much less than 1 is due to the large hierarchy between the mass scale and the scale of the scalar potential separating the false and true vacua, see eqs. (2.20) and (2.21). This leads to the hierarchy between the mass and the temperature at which the core of the sphaleron reaches outside, $\lambda_{HH,0} \gg m$. To prevent the sphaleron from escaping the BH vicinity, the barrier must be such that $q\lambda_{HH,0} \gtrsim m$ which is already achieved at $q \ll 1$. The situation is different in the four-dimensional model studied in appendix B.2, since there the sphaleron core is of the size of the Compton wavelength and reaches outside at $\lambda \sim m$. Hence, the value $q \sim 1$ corresponding to the Schwarzschild background is still not enough to confine the solution.

3.3 Decay probability

Let us now discuss the decay rate. We start from the low-temperature case when the bounce forms in the near-horizon region. The expression for the suppression of the Hartle–Hawking bounce for general values of $b_{HH} \leq 1$ and $x_{HH} < 0$ was derived in [41] and reads,[8]

$$B_{HH,\text{low-}\lambda} = \frac{4\pi}{\mathrm{g}^2}\left(\ln\left[\frac{4\lambda^2}{\kappa b_{HH}}\right] - 2\lambda x_{HH} - 4\right). \tag{3.18}$$

The derivation is insensitive to the shape of the potential for linear modes in the transition region $|x| \lesssim \lambda^{-1}$ and, hence, this formula is readily applicable to our model. Using eq. (3.3),

[8] Corrections to this formula are of order $\mathrm{g}^{-2} \times o(1)$.

we obtain

$$B_{HH,\text{low-}\lambda} = \frac{16\pi}{\mathrm{g}^2}\left(\ln\frac{\lambda}{\sqrt{\kappa}} - \frac{\lambda}{m+q\lambda}\right), \tag{3.19}$$

where, for simplicity, we have kept only the logarithmically enhanced terms. This expression is valid as long as the core of the bounce or sphaleron fits entirely into the near-horizon region, i.e., as long as

$$\lambda \lesssim \lambda_{HH,1} \equiv \frac{m}{2-a}\ln\frac{m}{\sqrt{\kappa}}, \tag{3.20}$$

where a is defined in eq. (3.13).

At higher temperature the vacuum decay proceeds via thermal jumps over the sphaleron which is the saddle-point of the energy barrier separating the vacua. The corresponding Boltzmann suppression is

$$B_{HH,\text{high-}\lambda} = \frac{2\pi E_{\text{sph}}}{\lambda}. \tag{3.21}$$

To find the sphaleron energy E_{sph}, we rewrite the general expression for it using integration by parts and equation of motion (3.6):

$$\begin{aligned} E_{\text{sph}} &= \frac{1}{\mathrm{g}^2}\int_{-\infty}^{+\infty}\mathrm{d}x\left(\frac{1}{2}\varphi'^2_{\text{sph}} + \frac{1}{2}(m^2\Omega + q\lambda\Omega')\varphi^2_{\text{sph}} - 2\kappa\Omega(\mathrm{e}^{\varphi_{\text{sph}}}-1)\right) \\ &= \frac{1}{\mathrm{g}^2}\int_{-\infty}^{+\infty}\mathrm{d}x\,\kappa\Omega\Big((\varphi_{\text{sph}}-2)\mathrm{e}^{\varphi_{\text{sph}}}+2\Big). \end{aligned} \tag{3.22}$$

Next, we substitute here the solution from the previous subsection (3.8), (3.9) in the case when the sphaleron sits on the dilaton barrier and use eqs. (3.13) and (3.16). Keeping only the leading logarithmically enhanced terms, we obtain

$$E_{\text{sph}} \simeq \frac{2(m+q\lambda)}{\mathrm{g}^2}\Big(\ln\frac{m}{\sqrt{\kappa}}\Big)^2. \tag{3.23}$$

This gives us the sphaleron energy up to

$$\lambda \lesssim \lambda_{HH,2} \equiv \frac{m}{q} = \frac{m}{a}\ln\frac{m}{\sqrt{\kappa}}. \tag{3.24}$$

As discussed before, at yet higher temperatures there are no sphalerons at finite distance from the BH. The height of the energy barrier separating the false and true vacua is then given by the energy of the flat-space sphaleron in the asymptotic region $x \to +\infty$, which is obtained by substituting (3.9) into (3.22) and taking the limit $x_{\text{sph,R}} \to +\infty$. This yields,

$$E^{\text{flat}}_{\text{sph}} \simeq \frac{4m}{\mathrm{g}^2}\Big(\ln\frac{m}{\sqrt{\kappa}}\Big)^2. \tag{3.25}$$

Substituting these results into eq. (3.21), we arrive at

$$B_{HH,\text{high-}\lambda} \simeq \begin{cases} \frac{4\pi(m+q\lambda)}{g^2\lambda}\left(\ln\frac{m}{\sqrt{\kappa}}\right)^2 , & \lambda_{HH,1} < \lambda < \lambda_{HH,2} \\ \frac{8\pi m}{g^2\lambda}\left(\ln\frac{m}{\sqrt{\kappa}}\right)^2 , & \lambda_{HH,2} < \lambda \end{cases} \tag{3.26}$$

At $\lambda = \lambda_{HH,1}$ this expression matches smoothly (both the function and its first derivative) to the low-temperature suppression (3.19). The suppression at this temperature is one-half of the suppression for tunneling in Minkowski spacetime (2.25). On the other hand, at $\lambda = \lambda_{HH,2}$ the suppression has a break (although it is still continuous). This is due to the abrupt run-away of the sphaleron to infinity.

We plot the suppression of the Hartle–Hawking vacuum decay in Fig. 8, where we compare it to the suppression of decay in thermal bath at the same temperature in the absence of BH. The latter was calculated in [41] and reads

$$B_{\text{th}}^{\text{flat}} \simeq \begin{cases} \frac{16\pi}{g^2}\left(\ln\frac{\lambda}{\sqrt{\kappa}} - \frac{\lambda}{2m}\right) , & \lambda < \lambda_0 \\ \frac{8\pi m}{g^2\lambda}\left(\ln\frac{m}{\sqrt{\kappa}}\right)^2 , & \lambda_0 < \lambda \end{cases} \tag{3.27}$$

where λ_0 is defined in eq. (3.10). We see that the BH provides an additional enhancement of the decay rate in a range of temperatures, but in the high temperature limit the catalyzing effect due to curved geometry disappears. Of course, at $\lambda \to \infty$ the suppression vanishes, as expected in a thermal state.

Let us make an observation that will be important in what follows. The sphaleron transition rate can be found using a simple stochastic picture [41]. At high temperature the occupation numbers of the low-lying modes are large and the field experiences large — essentially classical — fluctuations with a long correlation length $\sim m^{-1}$. From time to time these fluctuations will throw the field over the barrier separating the false and true vacua. The rate of such events can be estimated as

$$\Gamma_{HH,\text{high-}\lambda} \sim \exp\left(-\frac{\varphi_{\max}^2}{2(\delta\varphi)_{HH}^2}\right) , \tag{3.28}$$

where $\varphi_{\max}$ is the value of the field at the maximum of the scalar potential (2.21) and $(\delta\varphi)_{HH}^2$ is the variance of the fluctuations. In deriving eq. (3.28) we assumed that the fluctuations are Gaussian. This is a good approximation in our model since the scalar potential is essentially quadratic at $\varphi < \varphi_{\max}$ and hence the field is free as long as its amplitude does not exceed $\varphi_{\max}$.

The variance $(\delta\varphi)_{HH}^2$ at the position x can be found from the coincidence limit of the Green's function, upon subtraction of the Green's function in empty space to remove the ultraviolet divergence,

$$(\delta\varphi)_{HH}^2 = g^2 \lim_{t\to 0,\, x'\to x} \left[\mathcal{G}_{HH}(t,x';0,x) - \mathcal{G}_F(t,x';0,x)\right] . \tag{3.29}$$

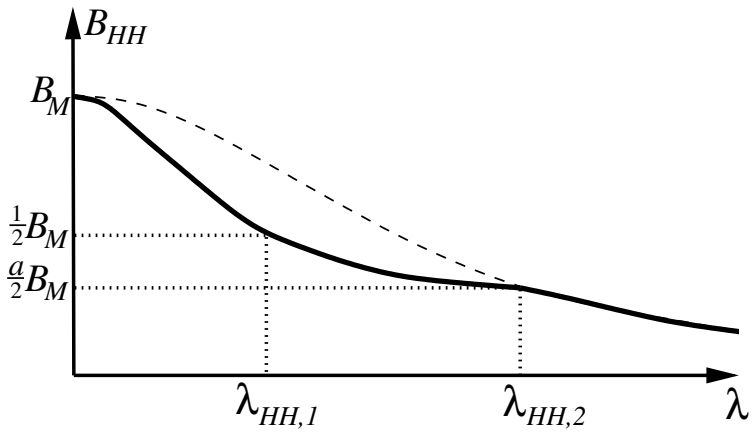


Figure 8: Exponential suppression of the Hartle–Hawking vacuum decay as a function of BH temperature $T_{BH} = \lambda/(2\pi)$ (solid) vs. suppression of the vacuum decay in a thermal bath with the same temperature in the absence of BH (dashed). At low temperature $\lambda < \lambda_{HH,1}$ decay proceeds via tunneling in the near-horizon region, at $\lambda_{HH,1} < \lambda < \lambda_{HH,2}$ via sphaleron transitions in the BH vicinity, and at $\lambda_{HH,2} < \lambda$ via sphaleron transitions far from BH. The critical temperatures marking the boundaries of different regimes are given by eqs. (3.20) and (3.24). We work in the regime of weak dilaton barrier.

From the expressions for the Hartle–Hawking Green's function to the right of the barrier, eq. (C.12), we see that the variance changes between

$$(\delta\varphi)^2_{HH} \simeq \frac{\mathrm{g}^2\lambda}{2\pi(m+q\lambda)} \quad \text{at } x = 0 \tag{3.30}$$

and

$$(\delta\varphi)^2_{HH} \simeq \frac{\mathrm{g}^2\lambda}{2\pi m} \quad \text{at } x \to +\infty\,. \tag{3.31}$$

Note that for $\lambda < \lambda_{HH,2}$ the fluctuations are larger in the vicinity of the BH which implies that the transitions will predominantly occur in this vicinity. However, for $\lambda > \lambda_{HH,2}$ the amplitude of fluctuations near the BH is suppressed compared to fluctuations at infinity. This is an effect of the high dilaton barrier for modes at $x = 0$ — the field gets repelled from the BH. In this case the transitions at infinity will be preferred, which confirms our earlier findings about the absence of sphaleron at finite x at these temperatures.

Substituting the maximal of the two expressions (3.30), (3.31) into eq. (3.28), we obtain

$$\Gamma_{HH,\text{high-}\lambda} \sim \begin{cases} \exp\left[-\frac{4\pi(m+q\lambda)}{\mathrm{g}^2\lambda}\left(\ln\frac{m}{\sqrt{\kappa}}\right)^2\right], & \lambda < \lambda_{HH,2} \\ \exp\left[-\frac{8\pi m}{\mathrm{g}^2\lambda}\left(\ln\frac{m}{\sqrt{\kappa}}\right)^2\right], & \lambda > \lambda_{HH,2} \end{cases} \tag{3.32}$$

which coincides with eq. (3.26). The stochastic approach is particularly useful when construction of the actual semiclassical solution is problematic. In the next section we will use it to estimate the rate of Unruh vacuum decay at high temperature.

4 Decay of the Unruh vacuum

We now turn to the main topic of this work — decay of the Unruh vacuum. We focus on the case of weak dilaton barrier, $a < 1$, where a is defined in eq. (3.13). As explained in sec. 3, in this regime the transitions from the Hartle–Hawking state proceed in close analogy with the four-dimensional case. It is reasonable to expect that the same is true for the Unruh vacuum.

Far from the BH, the Unruh vacuum corresponds to a flux of thermal radiation whose spectrum is reduced by the temperature-dependent barrier. Hence, we expect transitions far from BH to be more suppressed than in the model without the barrier studied in [41]. Close to the horizon, by analogy with the Hartle–Hawking case, we expect that the Unruh bounce exists in a certain range of BH temperatures and disappears at a high enough temperature.

4.1 Tunneling near horizon

To find the Unruh bounce in the BH vicinity, we have to solve eq. (2.13) with $\Omega = \mathrm{e}^{2\lambda x}$ along the contour $\mathscr{C}$ shown in Fig. 2 and satisfy the boundary condition imposed by the Unruh vacuum.[9] In the core region of the bounce the field equation reduces to eq. (3.1). The tail of the bounce is determined by the time-ordered Unruh Green's function $\mathcal{G}_U$ computed in the BH vicinity. Overall, we have [41]

$$\varphi_{\mathrm{b}}\big|_{\mathrm{core}} = \ln\left[\frac{4\lambda^2 b_U}{\kappa\left(-2\lambda(v-x_U)\,\mathrm{sh}\left(\frac{\lambda}{2}(u+x_U)\right)+b_U\mathrm{e}^{\frac{\lambda}{2}(u+x_U)}\right)^2}\right] - 2\lambda x \tag{4.1a}$$

$$\varphi_{\mathrm{b}}\big|_{\mathrm{tail}} = 8\pi\mathcal{G}_U(t,x;0,x_U) \tag{4.1b}$$

Here we defined $u = t - x$, $v = t + x$. The core expression (4.1a) has been built in such a way that in the linearized regime its u- and v-dependent parts match the corresponding terms in the Green's function. The parameter x_U determines the position of the center of the bounce

[9] As in the Hartle–Hawking case, $\mathscr{C}$ can be deformed into the contour $\mathscr{C}'$ with a part in the Euclidean time domain, see Fig. 5. This facilitates the matching procedure and is legitimate since the deformation does not intersect singularities of the bounce. Note, however, that unlike the Hartle–Hawking case, the Unruh bounce is not real in Euclidean time.

and b_U is found from matching the constant parts of (4.1a) and (4.1b). For simplicity, we will keep in this matching only the terms enhanced by the large ratio λ/m. This yields

$$b_U = \bar{b}_U \mathrm{e}^{-2\lambda x_U} , \qquad \bar{b}_U = \frac{\kappa}{4m^2} \exp\left\{ \frac{4\lambda}{\pi m} \mathcal{H}\Big(\frac{q\lambda}{m}\Big) \right\} , \tag{4.2}$$

where the function $\mathcal{H}$ is defined in eq. (C.14a) and plotted in Fig. 14. As in the Hartle–Hawking case, we obtain a one-parameter family of solutions parameterized by x_U. Again, this is an artifact of our approximation of the near-horizon geometry by the Rindler spacetime. One expects that taking into account the deviation of BH metric from Rindler will remove the degeneracy [41].

For the applicability of the matching procedure the bounce core should be smaller than the tail, which amounts to the requirement

$$\bar{b}_U \lesssim 1 . \tag{4.3}$$

More careful matching conditions can be found in [41], but they are not important for what follows. Inequality (4.3) translates into the upper bound on the BH temperature,

$$\lambda < \lambda_U \equiv \frac{y_c m}{a} \ln \frac{m}{\sqrt{\kappa}} , \tag{4.4}$$

where y_c is the solution of the equation

$$y_c \mathcal{H}(y_c) = \frac{\pi a}{2} . \tag{4.5}$$

Note that this solution exists for $a < 1$ due to the asymptotics of the function $\mathcal{H}$, eqs. (C.15), (C.16). At $\lambda > \lambda_U$, the bound (4.3) is violated and the matching procedure breaks down. At the same time, the Liouville core of the Unruh bounce stops fitting the near-horizon region. By analogy with the Hartle–Hawking case, we expect that further growth of temperature drives the vacuum decay site across the gravitational barrier and to the flat-space region on the right. We were not able to find explicitly the corresponding bounce solutions. Nevertheless, we will see below that the vacuum decay rate in this regime can be estimated using the stochastic picture.

Presently, let us return to the near-horizon bounces and compute their tunneling suppression. A general expression for it was derived in [41] and reads as follows

$$B_{U,\text{low-}\lambda} = \frac{4\pi}{\mathrm{g}^2} \left(\ln \left[\frac{4\lambda^2}{\kappa \bar{b}_U} \right] - 4 \right) . \tag{4.6}$$

It is not sensitive to the shape of the mode potential (2.11) in the transition region $|x| \lesssim \lambda^{-1}$ and, hence, is applicable to our model. Keeping only the logarithmically enhanced terms, we obtain

$$B_{U,\text{low-}\lambda} = \frac{16\pi}{\mathrm{g}^2} \left(\ln \sqrt{\frac{\lambda m}{\kappa}} - \frac{\lambda}{\pi m} \mathcal{H}\Big(\frac{q\lambda}{m}\Big) \right) . \tag{4.7}$$

For $q = 0$, using eq. (C.15), we recover the suppression for the model without dilaton barrier [41],

$$B_{U,\text{low-}\lambda}\Big|_{q=0} = \frac{16\pi}{\mathrm{g}^2}\left(\ln\sqrt{\frac{\lambda m}{\kappa}} - \frac{8\lambda}{3\pi m}\right) . \tag{4.8}$$

For all values of q corresponding to weak barrier the suppression monotonically decreases with temperature from the flat-space value B_M (eq. (2.25)) at $\lambda \simeq m$ down to $B_M/2$ at $\lambda = \lambda_U$, at which point the near-horizon bounces cease to exist.

4.2 Stochastic jumps at high temperature

Following the lessons learned from the Hartle–Hawking case, we expect that the Unruh vacuum decay at $\lambda > \lambda_U$ proceeds via large stochastic fluctuations kicking the field over the maximum of the scalar potential $\varphi_{\max}$. The corresponding decay rate is

$$\Gamma_{U,\text{high-}\lambda} \sim \exp\left(-\frac{\varphi_{\max}^2}{2(\delta\varphi)_U^2}\right) . \tag{4.9}$$

The variance of the fluctuations is estimated from the coincidence limit of the Green's function,

$$(\delta\varphi)_U^2 = \mathrm{g}^2 \lim_{t\to 0,\, x'\to x} \left[\mathcal{G}_U(t,x';0,x) - \mathcal{G}_F(t,x';0,x)\right] , \tag{4.10}$$

where for $\mathcal{G}_U$ we use the expressions (C.18), (C.19) valid to the right of the barrier at $x = 0$. Focusing on the dominant terms containing the enhancement factor λ/m, we see that the variance monotonically decreases from the value

$$(\delta\varphi)_U^2\Big|_{x\to 0} = \frac{\mathrm{g}^2\lambda}{2\pi^2 m}\mathcal{H}\Big(\frac{q\lambda}{m}\Big) \tag{4.11}$$

in the vicinity of BH down to

$$(\delta\varphi)_U^2\Big|_{x\to +\infty} = \frac{\mathrm{g}^2\lambda}{2\pi^2 m}\tilde{\mathcal{H}}\Big(\frac{q\lambda}{m}\Big) \tag{4.12}$$

far away from it. The functions $\mathcal{H}(y)$ and $\tilde{\mathcal{H}}(y)$ are defined in eqs. (C.14a) and (C.20a), respectively and are plotted in Fig. 14. The characteristic distance from the BH at which the amplitude of the fluctuations changes is of order $(q\lambda)^{-1}$. This is illustrated on the left plot in Fig. 9.

For not-so-large temperature $\lambda \sim m/q$, the neighborhood of the BH with large fluctuations is of size m^{-1}, sufficient to accommodate the flat-space sphaleron. At such temperature the vacuum decay will be dominated by sphaleron transitions in the BH vicinity.

At yet higher temperature, $\lambda \gg m/q$, the size of the region with enhanced fluctuations shrinks. However, also the variance of the fluctuations levels out throughout the whole space,

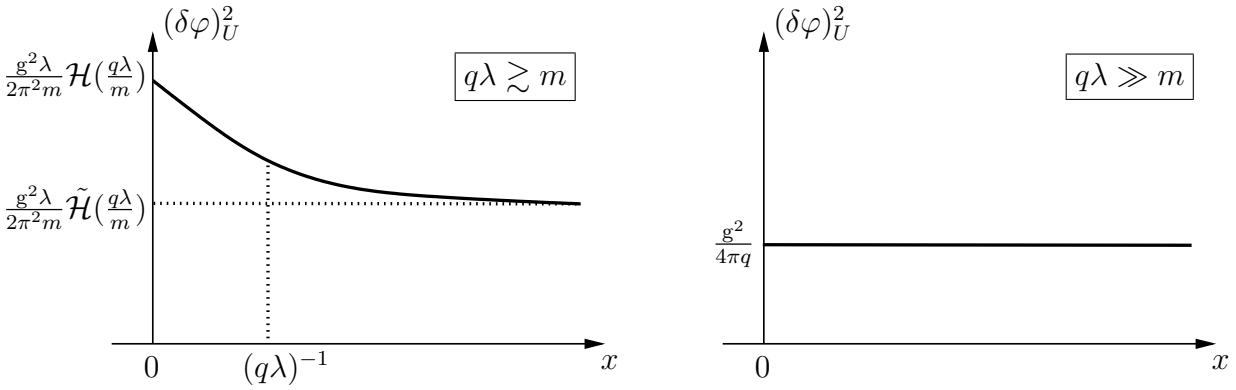


Figure 9: Variance of the field fluctuations in the Unruh vacuum outside BH as a function of the space coordinate. *Left:* moderate BH temperature $q\lambda \gtrsim m$. *Right:* limit of very high temperature $q\lambda \gg m$.

because the asymptotics of the functions $\mathcal{H}(y)$ and $\tilde{\mathcal{H}}(y)$ at $y \gg 1$ coincide, see eqs. (C.16), (C.22). We obtain that in the high-temperature limit the variance is finite and equals

$$(\delta\varphi)^2_U\Big|_{q\lambda\gg m} = \frac{g^2}{4\pi q} \tag{4.13}$$

irrespective of the position x, see Fig. 9, right plot.[10] This constancy of the variance has clear physical interpretation: the flux of particles emitted by the BH and producing the fluctuations remains constant at arbitrary distance from the BH due to the two-dimensional nature of the model. Thus, the sphaleron transitions can now happen with the same probability anywhere in space.

Putting everything together, we estimate the rate of the Unruh vacuum decay at any temperature above λ_U as

$$\Gamma_{U,\text{high-}\lambda} \sim \exp\left[-\frac{4\pi^2 m}{g^2\lambda}\left(\mathcal{H}\Big(\frac{q\lambda}{m}\Big)\right)^{-1}\left(\ln\frac{m}{\sqrt{\kappa}}\right)^2\right]. \tag{4.14}$$

Remarkably, this expression matches the low-temperature suppression (4.7) at $\lambda = \lambda_U$ up to the first derivative with respect to λ. This supports the stochastic picture of vacuum decay advocated above.

Crucially, the exponential suppression of decay persists even in the limit of infinite BH temperature,

$$\Gamma_{U,\lambda\to\infty} \sim \exp\left[-\frac{8\pi a}{g^2}\ln\frac{m}{\sqrt{\kappa}}\right]. \tag{4.15}$$

[10]The subdominant terms in the Green's function (C.18), (C.19) lead to a slight suppression of $(\delta\varphi)^2_U$ at $x = 0$ compared to the asymptotics at infinity. However, the subdominant effects are likely beyond the validity of the rough estimates (4.9), (4.10).

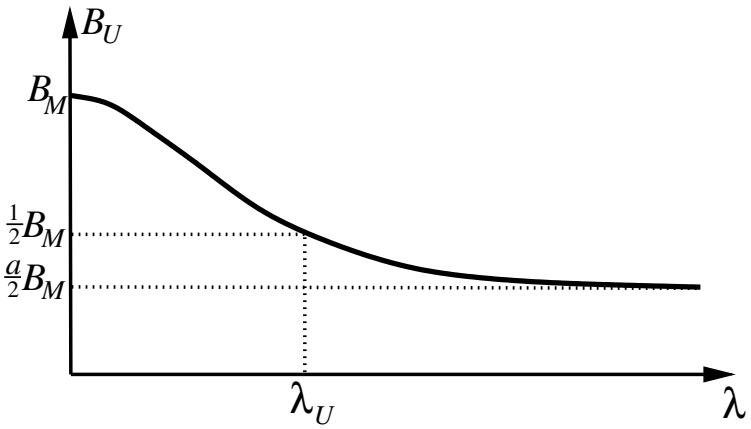


Figure 10: Exponential suppression of the Unruh vacuum decay as a function of BH temperature $T_{BH} = \lambda/(2\pi)$. Decay proceeds via tunneling in the near-horizon region at $\lambda < \lambda_U$, whereas at $\lambda > \lambda_U$ it is mediated by stochastic jumps in the vicinity and far away from BH. The critical temperature λ_U is given by eq. (4.4). The suppression approaches a non-zero constant in the limit $\lambda \to \infty$. We consider the case of weak dilaton barrier, $0 < a < 1$.

This is in striking contrast to the Hartle–Hawking case and is a direct consequence of the lack of particles in the Unruh flux compared to the thermal state. We believe this property to be universal and valid also for BHs in higher dimensions. It hinges on the presence of the centrifugal barrier reducing the outgoing flux through non-trivial greybody factors. We plot our results for the Unruh vacuum decay suppression in Fig. 10.

One point needs to be discussed before closing this section. At very high BH temperature the Unruh flux is dominated by relativistic modes with high momenta $k \sim q\lambda \gg m$ that most efficiently escape through the barrier. Thus, the correlation length of fluctuations $l_{\rm corr} \sim k^{-1}$ is much shorter than m^{-1} and further decreases with temperature. One may ask if this leads to additional suppression of transitions compared to eq. (4.15), so that the actual suppression grows with temperature. We now show that this is not the case, at least in our two-dimensional setup.[11]

To this end, let us look at the spectrum of particles in the Unruh flux. Far away from the BH particle occupation numbers are given by the product of the Bose–Einstein distribution and the transmission coefficient through the barrier,

$$n_k = \frac{1}{\mathrm{e}^{2\pi\omega/\lambda} - 1} \cdot \frac{k}{\omega} |\gamma_\omega|^2 \,, \tag{4.16}$$

where ω is the particle energy, $\omega = \sqrt{k^2 + m^2}$, the transmission amplitude γ_ω is defined in eq. (C.3), and the factor k/ω appears due to the different normalization of plane waves

[11] In higher dimensions the suppression may actually increase at $\lambda \to \infty$ due to the drop of the particle flux according to the inverse area law at finite distance from the BH, see the discussion in sec. 5.

on the left and on the right from the barrier. Although the relevant particle energies are higher than m, they are still well below λ (recall that $q \ll 1$). Thus, we can expand the Bose–Einstein factor at $\omega \ll \lambda$ and use the formula (C.7b) for γ_ω. We obtain,

$$n_k = \frac{2\lambda k}{\pi\big((\omega+k)^2 + (q\lambda)^2\big)} \,. \tag{4.17}$$

As expected, this describes a broad spectrum of particles centered at $\omega \approx k \approx q\lambda/2$.

Let us perform a boost to the rest frame of particles moving with the central momentum. In terms of the momentum and energy in the new frame the occupation numbers read

$$n_{k'} = \frac{m(\omega'+k')}{\pi q\big((\omega'+k')^2 + m^2\big)} \,. \tag{4.18}$$

We see that in the boosted frame the Unruh flux represents a collection of soft particles with momenta $k' \sim m$. Thus, we arrive at the following physical picture. In the reference frame comoving with the radiation, the flux consists of soft modes with high occupation numbers $n_{k'} \sim 1/q \gg 1$. Collisions between these modes lead to stochastic fluctuations at the scales $k'^{-1} \sim m^{-1}$ and induce sphaleron transitions in this frame without any extra exponential suppression on top of eq. (4.15). Note that from the viewpoint of the original "laboratory" frame connected to the BH, the produced sphalerons are highly boosted.

5 Conclusions

In this paper, we studied a toy model of vacuum decay induced by a BH. To model the BH background, we used the theory of two-dimensional dilaton gravity. In this background, we considered the massive scalar field with the negative Liouville potential. To emulate the four-dimensional centrifugal barrier for massive scalar modes, we added the temperature-dependent scalar-dilaton coupling. This coupling is a new ingredient compared to the model studied in our previous work [41], and it brings us one step closer to a realistic four-dimensional system. In this model, we first studied Hartle–Hawking vacuum decay, for which our results can also be obtained by applying the standard Euclidean instanton method. In particular, we found that in the high-temperature limit vacuum transitions occur in the asymptotically-flat region and are not suppressed. This is consistent with previous works on BH catalysis [5–8].

We then turned to the Unruh vacuum and found that the presence of the barrier changes drastically the exponential suppression of the Unruh vacuum at high temperatures. This is because the barrier reduces the flux of particles emitted by the BH that escape its immediate vicinity. Unlike the Hartle–Hawking case, the suppression of the Unruh vacuum decay does not disappear even in the high-temperature limit; instead, it tends to constant. This is the main result of our study.

At low temperature the Unruh vacuum decay proceeds via tunneling in the BH vicinity. We found analytically the corresponding bounce solution and tunneling rate. At high temperature, the decay regime changes to stochastic jumps over the sphaleron separating the vacua, and the decay site shifts to the outer region. Thanks to the features of our model, we were able to apply a simple stochastic estimate to find the decay rate in this regime. The stochastic approach can, in principle, work in more general situations, but will require full-fledged numerical simulation of the classical field dynamics [62–65] (see also [66–68]). The implementation of such a simulation would be useful since it would allow one to go beyond the special exactly-solvable model that was studied here.

Note that one important ingredient of the four-dimensional setup — the dilution of the Hawking flux as it moves away from the BH — is still not captured by our model. Hence, one can expect further suppression of the decay probability of the Unruh vacuum at high BH temperature. Indeed, consider a BH with $T_{BH} \gg m$ and disregard the effect of the centrifugal barrier, allowing the occupation numbers of soft modes with $\omega \sim m$, which are relevant for the decay, to be thermally enhanced close to the horizon, $n_{\rm soft}\big|_{r\sim r_h} \sim T_{BH}/m$. Of course, this is an overestimate as the greybody factors strongly suppress $n_{\rm soft}$. Even in this case, the occupation numbers become small already at the distance m^{-1},

$$n_{\rm soft}\big|_{r\sim m^{-1}} \sim \frac{T_{BH}}{m}\cdot\left(\frac{r_h}{m^{-1}}\right)^2 \sim \frac{m}{T_{BH}} \ll 1\,.$$

Thus, there are simply not enough modes to generate a classical field fluctuation that would trigger the decay [11, 52]. One can reasonably expect that the largest catalyzing effect is achieved when the size of the BH is of order m^{-1}. This expectation needs to be confirmed by explicit calculation, using, e.g., the method of [41]. We leave this for future work.

Acknowledgments

We are grateful to Matthew Johnson, Kohei Kamada and Naritaka Oshita for useful discussions. The work was in part supported by the Department of Energy Grant DE-SC0011842 (A.S.). The work was partially supported by the Russian Foundation for Basic Research grant 20-02-00297 (S.S.). The work of S.S. is supported by the Natural Sciences and Engineering Research Council (NSERC) of Canada. Research at Perimeter Institute is supported in part by the Government of Canada through the Department of Innovation, Science and Economic Development Canada and by the Province of Ontario through the Ministry of Colleges and Universities.

A Dilaton black holes

We consider the following action of dilaton gravity in two dimensions [53]

$$S_{\rm DG} = \int \mathrm{d}^2x\sqrt{-g}\,\mathrm{e}^{-2\phi}\left(R + 4(\nabla_\mu\phi)^2 + 4\lambda^2\right)\ . \tag{A.1}$$

Here R is the scalar curvature and λ is a constant parameter. The theory admits a one-parameter family of BH solutions with the metric determined by

$$\mathrm{d}s^2 = -\Omega(r)\mathrm{d}t^2 + \frac{\mathrm{d}r^2}{\Omega(r)}\ . \tag{A.2}$$

The function Ω and the dilaton field ϕ are given by

$$\Omega(r) = 1 - \frac{M}{2\lambda}\mathrm{e}^{-2\lambda r}\ , \quad \phi = -\lambda r\ . \tag{A.3}$$

The mass of a BH is M and its horizon radius is

$$r_h = \frac{1}{2\lambda}\ln\frac{M}{2\lambda}\ . \tag{A.4}$$

Introducing the tortoise coordinate

$$x = \frac{1}{2\lambda}\ln\left[\mathrm{e}^{2\lambda r} - \mathrm{e}^{2\lambda r_h}\right] - r_h\ , \tag{A.5}$$

and re-expressing Ω and ϕ as functions of x, we obtain eqs. (2.2) and (2.4).

Throughout the paper, we neglect the back-reaction of the tunneling field φ on the geometry. This is justified if the gravitational coupling $\mathrm{e}^{2\phi}$ is small compared to the scalar coupling g from eq. (2.5). Its maximal value in the BH exterior is reached at the horizon,

$$\mathrm{e}^{2\phi}\Big|_{r=r_h} = \frac{2\lambda}{M}\ . \tag{A.6}$$

This imposes a restriction on the parameter M_0 introduced in eq. (2.10),

$$M_0^2 \gg \frac{\lambda^2}{\mathrm{g}^2}\ . \tag{A.7}$$

This can always be satisfied for large enough M_0. Note that if we allow $q = 2Q/M_0^2$ to be of order one, the non-minimal coupling of the scalar to the dilaton must be large,

$$Q \gg \frac{\lambda^2}{\mathrm{g}^2}\ . \tag{A.8}$$

However, this is not a problem since Q enters the action in the combination $Q\mathrm{e}^{2\phi}$ which is bounded from above by $q\lambda^2$.

B Schwarzschild black hole in four dimensions

B.1 Mode potential

Let us see how the greybody factors arise in the theory obtained from four dimensions by a spherical reduction. Consider a free massive scalar χ in four dimensions,

$$S = \int \mathrm{d}^4x\sqrt{-g}\left(-\frac{1}{2}g^{\mu\nu}\partial_\mu\chi\partial_\nu\chi - \frac{m^2\chi^2}{2}\right) , \tag{B.1}$$

and adopt the Schwarzschild metric,

$$\mathrm{d}s^2 = -\Omega(r)\mathrm{d}t^2 + \frac{\mathrm{d}r^2}{\Omega(r)} + r^2\mathrm{d}\Omega_2^2 , \tag{B.2}$$

where $\mathrm{d}\Omega_2^2$ is the line element of a unit 2-sphere and

$$\Omega(r) = 1 - \frac{r_h}{r} . \tag{B.3}$$

Let us make the field redefinition

$$\varphi = r\chi \tag{B.4}$$

and introduce the tortoise coordinate

$$x = r + r_h \ln\left[\frac{r}{r_h} - 1\right] . \tag{B.5}$$

Then, upon restricting to spherically-symmetric configurations, $\chi = \chi(t, r)$, changing the variables in the action (B.1) according to eqs. (B.4) and (B.5) and integrating by parts, we obtain

$$S = 4\pi\int \mathrm{d}t\mathrm{d}x\left(\frac{1}{2}\dot{\varphi}^2 - \frac{1}{2}\varphi'^2 - \frac{1}{2}\left(m^2\Omega + \frac{\Omega'}{r}\right)\varphi^2\right) , \tag{B.6}$$

where dot (prime) denotes derivative with respect to t (x) and $r = r(x)$ is the inverse of eq. (B.5).

From eq. (B.6) we read off the effective potential for spherically-symmetric scalar modes (see Fig. 11 for illustration),

$$U_{\text{eff}}^{(4d)} = m^2\Omega + \frac{\Omega'}{r} . \tag{B.7}$$

This should be compared with the effective potential in the dilaton BH (2.9). Let us focus on the second term that gives rise to the potential barrier. In the region $x \sim 0$, where the barrier achieves its maximum, r is of order the Schwarzschild radius, $r \sim r_h$. The latter is related to the BH temperature as $r_h = (2\lambda)^{-1}$. Hence, to mimic the Schwarzschild greybody factors with two-dimensional dilaton gravity, the coefficient $2Q/M$ in eq. (2.9) must be $\propto \lambda$. This is achieved by imposing the condition (2.10).

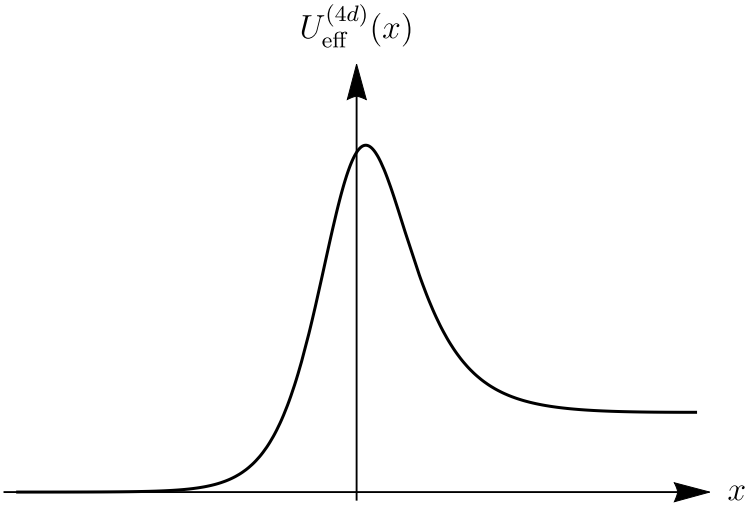


Figure 11: Effective potential for spherically symmetric linear massive modes in the four-dimensional Schwarzschild geometry.

Comparing the near-horizon asymptotics of the two potentials, we see that they agree at $q = 2$. However, as explained in the main text, the physics of vacuum decay is qualitatively similar already at much lower values of q, and the range (2.12) suffices. The large distance asymptotics of eqs. (2.11) and (B.7) are different because of the different form of the function $\Omega(x)$ and the presence of the function $r = r(x)$ in the denominator of the second term in eq. (B.7). The latter comes from the area growth in four dimensions. Removing it, i.e., replacing $r(x) \mapsto r_h$, makes the two potentials completely analogous. In particular, in the near-horizon region the area factor is not important.

B.2 Hartle–Hawking sphaleron

Here we study the Hartle–Hawking sphaleron in the four-dimensional Schwarzschild background for a scalar theory with inverted quartic potential. Consider the action

$$S = \int \mathrm{d}^4x\sqrt{-g}\left(-\frac{1}{2}g^{\mu\nu}\partial_\mu\chi\partial_\nu\chi - \frac{1}{2}m^2\chi^2 + \frac{\mathrm{g}^2}{4}\chi^4\right) , \tag{B.8}$$

where $\mathrm{g}^2 > 0$. We redefine the coordinates and the field variable χ as in appendix B.1, further rescale $\varphi \mapsto \varphi/\mathrm{g}$, and restrict to spherically-symmetric configurations. In this way, we arrive at

$$S = \frac{4\pi}{\mathrm{g}^2}\int \mathrm{d}t\mathrm{d}x\left(\frac{1}{2}\dot{\varphi}^2 - \frac{1}{2}\varphi'^2 - \frac{1}{2}\left(m^2\Omega + \frac{\Omega'}{r}\right)\varphi^2 + \frac{\Omega}{4r^2}\varphi^4\right) , \tag{B.9}$$

where the conformal factor Ω is defined in eq. (B.3), and $r = r(x)$ is the inverse of eq. (B.5). One observes that the structure of this action closely resembles that of the two-dimensional

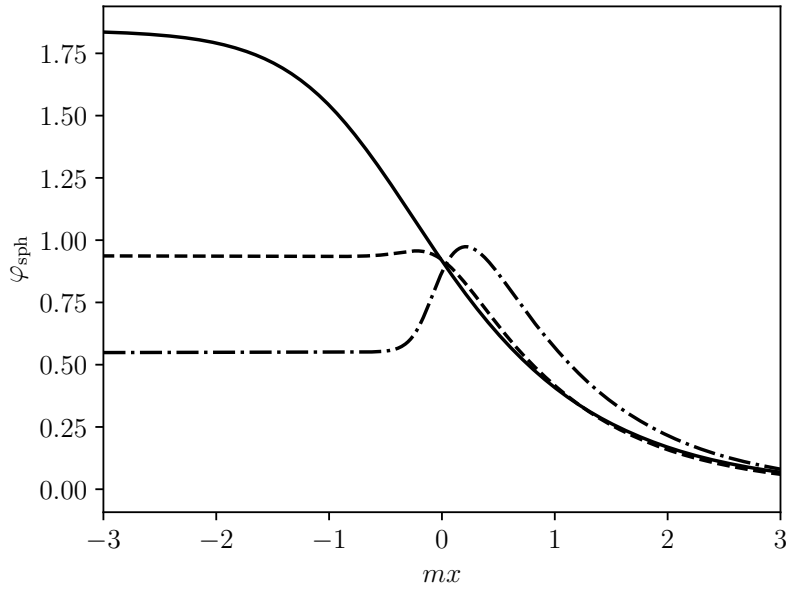


Figure 12: Profiles of the Hartle–Hawking sphaleron in the four-dimensional Schwarzschild background at different BH temperatures: $2\pi T_{BH} = 1.0m$ (solid), $3.5m$ (dashed), $7.0m$ (dash-dot).

model (2.6) studied in the main text. The important difference, however, is the explicit coordinate dependence of the interaction term.

The equation of motion for a static configuration is

$$\varphi''_{\rm sph} - \left(m^2\Omega + \frac{\Omega'}{r}\right)\varphi_{\rm sph} + \frac{\Omega}{r^2}\varphi^3_{\rm sph} = 0\,. \tag{B.10}$$

This must be supplemented with the boundary conditions,

$$\varphi_{\rm sph}(x \to -\infty) \to \text{const}\,, \quad \varphi_{\rm sph}(x \to \infty) \to 0\,. \tag{B.11}$$

The first condition reflects regularity of the Hartle–Hawking state at the horizon, and the second is the vacuum boundary condition away from the BH. Finally, the energy of the sphaleron reads

$$E_{\rm sph} = \frac{4\pi}{\mathrm{g}^2}\int_{-\infty}^{\infty}\mathrm{d}x\,\left(\frac{1}{2}\varphi'^2_{\rm sph} + \frac{1}{2}\left(m^2\Omega + \frac{\Omega'}{r}\right)\varphi^2_{\rm sph} - \frac{\Omega}{4r^2}\varphi^4_{\rm sph}\right)\,. \tag{B.12}$$

We solve eqs. (B.10) and (B.11) numerically. We are interested in the behavior of the sphaleron profile as the Schwarzschild radius r_h (or the BH temperature $T_{\rm BH} = 1/(4\pi r_h)$) varies. The sample plots are shown in Fig. 12. We see that at $r_h m \gtrsim 1$, the nonlinear core

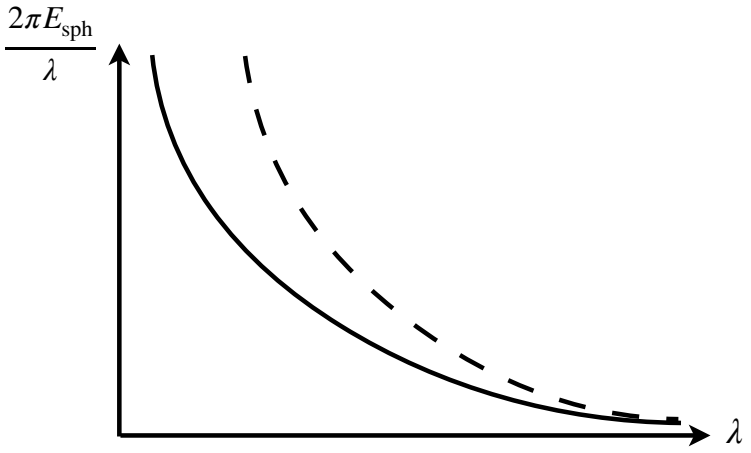


Figure 13: Suppression of the sphaleron transitions in the Hartle–Hawking vacuum as function of the BH temperature $T_{BH} = \lambda/(2\pi)$ (solid). The sphaleron energy $E_{\rm sph}$ is defined in eq. (B.12). Dashed line shows the sphaleron suppression in thermal bath at the same temperature in flat space.

of the solution is localized in the near-horizon region. On the other hand, at $r_h m \lesssim 1$, the core does not fit the BH neighborhood. Moreover, the function $\varphi_{\rm sph}(x)$ is not a monotonic function, with the maximum outside the near-horizon region.[12]

At small BH temperatures, the Hartle–Hawking sphaleron deviates from its flat counterpart. This is because the size of the BH r_h exceeds the characteristic size of the flat sphaleron which is $\propto m^{-1}$. In the opposite limit the BH is small and, as one can readily check, the sphaleron is insensitive to the curved geometry and tends asymptotically to the flat-space solution.

Finally, Fig. 13 shows the Boltzmann suppression factor $E_{\rm sph}/T_{\rm BH}$ in the BH background vs. the Boltzmann suppression at the same temperature in flat space. We see that the BH transition channel always dominates over the flat-space channel, although at $r_h m \gtrsim 1$ both are superseded by the transition via the flat-space periodic bounce [9].[13]

Thus, we draw two important conclusions. First, if the BH temperature is below the scale associated with the size of the sphaleron core (which is m^{-1} in this case), the nonlinear part of the sphaleron is localized in the near-horizon region; at higher BH temperature the sphaleron shifts outside. Second, in the large temperature limit the solution and the associated decay suppression tend to the ones in flat spacetime. Comparing with the two-dimensional model studied in the main text, we see that this qualitative behavior is reproduced in the regime of weak dilaton barrier, see sec. 3.2.

[12]The sphaleron profile is still monotonic if written in terms of the original field variable χ.

[13]It is known that the theory (B.8) in flat spacetime does not admit a finite-size bounce at zero temperature [69]. Periodic bounces, however, exist.

C Linear modes and Green's functions

Here we discuss some further properties of the potential (2.11) and of the linear modes in this potential. We also compute the Green's functions in the regions of interest. Our aim is to highlight differences between the model with the scalar-dilaton coupling and the model without the dilaton barrier studied in [41]. The reader is referred to Appendix B of that paper for more details.

C.1 Effective potential, modes and scattering coefficients

Consider the potential (2.11). When $2q\lambda^2 > m^2$, the barrier generated by the second term exceeds the asymptotics at positive x. The height of the barrier and its position are

$$U_{\max} = \frac{(2q\lambda^2 + m^2)^2}{8q\lambda^2} \,, \quad x_{\max} = \frac{1}{2\lambda} \ln\left[\frac{2q\lambda^2 + m^2}{2q\lambda^2 - m^2}\right] \,, \quad 2q\lambda^2 > m^2 \,. \tag{C.1}$$

The width of the region where the potential changes rapidly is

$$\Delta x \sim \lambda^{-1} \,. \tag{C.2}$$

As discussed in sec. 2.2, the mode equation (2.8) with potential (2.11) can be solved exactly in terms of the hypergeometric functions. Using the general solution, we construct a basis of orthogonal and delta-function normalizable modes $f_{L,\omega}$, $f_{R,\omega}$ for $\omega > m$. At $x \to \pm\infty$ the modes become plane waves. The modes $f_{L,\omega}$ are left-moving at large negative x, whereas the modes $f_{R,\omega}$ are right-moving at large positive x. Using the asymptotics of the modes $f_{R,\omega}$ we determine the reflection and transmission amplitudes of the potential (2.11),

$$f_{R,\omega} = \begin{cases} \mathrm{e}^{i\omega x} + \beta_\omega \, \mathrm{e}^{-i\omega x} \,, & x \to -\infty \\ \gamma_\omega \, \mathrm{e}^{ikx} \,, & x \to +\infty \end{cases} \tag{C.3}$$

where

$$k = \sqrt{\omega^2 - m^2} \,, \quad \omega > m \,. \tag{C.4}$$

These obey the unitarity constraint

$$|\beta_\omega|^2 + \frac{k}{\omega} |\gamma_\omega|^2 = 1 \,. \tag{C.5}$$

The asymptotics of $f_{L,\omega}$ are then also fully fixed in terms of β_ω and γ_ω.

At $0 < \omega < m$ only one family of the modes survives, which is exponentially damped at $x \to +\infty$. This can be obtained from the modes $f_{R,\omega}$ by analytic continuation

$$k \mapsto i\sqrt{m^2 - \omega^2} \equiv i\varkappa \,. \tag{C.6}$$

We will continue to denote this family by $f_{R,\omega}$, though, of course, there are no right-moving waves at large x in this case. The reflection and "transmission" amplitudes are still defined using eq. (C.3), but no longer obey the relation (C.5). Instead, we have $|\beta_\omega| = 1$.

We only need the expressions for β_ω and γ_ω at frequencies much below the temperature λ. In this limit, instead of using the exact hypergeometric mode functions, it is simpler to obtain the modes by approximating U_{eff} with a superposition of a step-function (corresponding to the first term in eq. (2.11)) and a δ-function (corresponding to the second term). One then finds

$$\beta_\omega = \frac{i(\omega - k) + q\lambda}{i(\omega + k) - q\lambda}\,, \qquad \omega \ll \lambda \tag{C.7a}$$

$$\gamma_\omega = \frac{2i\omega}{i(\omega + k) - q\lambda}\,, \qquad \omega \ll \lambda \tag{C.7b}$$

where we have assumed $q \ll 1$. The expressions (C.7) can be analytically continued from $\omega > m$ to $\omega < m$ with the replacement (C.6).

Let us note two properties of the amplitudes β_ω, γ_ω. First, at $q\lambda \ll \omega \ll \lambda$ one can neglect the term $q\lambda$ in eqs. (C.7) and we return to the case $q = 0$. Hence, $\omega \sim q\lambda$ is the characteristic frequency of the barrier. Second, in the opposite limit $\omega \to 0$ the reflection and transmission amplitudes behave as

$$|\beta_\omega| = 1\,, \quad |\gamma_\omega| = \frac{2\omega}{m + q\lambda}\,, \quad \omega \to 0\,. \tag{C.8}$$

We observe that the mass in $|\gamma_\omega|$ appears in the combination $m + q\lambda$. The interplay between the two terms in this combination governs various tunneling regimes, as discussed in the main text.

C.2 Green's functions in the asymptotic regions

Here we summarize the expressions for the Hartle–Hawking and Unruh Green's functions which we use in the main text, postponing their derivation to the next subsection. We only need their form when the two points x, x' are placed in the near-horizon or asymptotically-flat regions, where the mode functions $f_{L,\omega}$, $f_{R,\omega}$ are approximated by plane waves. To the former region we refer as "left" and to the latter as "right". The two asymptotics are separated by the region where the potential (2.11) changes rapidly. The width of this region is given in eq. (C.2). Hence, one can take

$$x, x' < 0\,, \qquad |x|, |x'| \gg \lambda^{-1} \qquad (\text{"left"}), \tag{C.9}$$

$$x, x' > 0\,, \qquad x, x' \gg \lambda^{-1} \qquad (\text{"right"}). \tag{C.10}$$

Furthermore, we need the Green's functions at "close separation". This means that we assume $|x-x'|$, $|t-t'|$ to be sufficiently small, so that the Green's functions are approximated by their short-distance asymptotics. The precise conditions are different for different cases and will be listed below for each case separately. We will use the superscript "close" to indicate that an expression is valid under this assumption.

All expressions below are derived under the conditions $m \ll \lambda$, $q \ll 1$. Note that no relation between m and $q\lambda$ is assumed. Using the time translation invariance of the BH background, we set $t' = 0$.

Hartle–Hawking Green's function (left):

$$\begin{aligned}\mathcal{G}_{HH}|_{\text{left}} = &-\frac{1}{4\pi}\ln\left[4\,\mathrm{sh}\left(\frac{\lambda}{2}(x-x'-t)\right)\mathrm{sh}\left(\frac{\lambda}{2}(x-x'+t)\right)+i\epsilon\right]\\ &-\frac{\lambda}{4\pi}(x+x')+\frac{\lambda}{2\pi(m+q\lambda)}\,.\end{aligned} \tag{C.11}$$

This expression is valid provided that eq. (C.9) is fulfilled and $|t| < |x+x'|$. No further assumptions about $|x-x'|$ or $|t|$ are needed. In the limit $q \to 0$, the Green's function reduces to the one in the model without the scalar-dilaton coupling [41]. We see that the only effect of the barrier is the replacement $m \mapsto m + q\lambda$ in the last term in this expression.

Hartle–Hawking Green's function (right):

$$\begin{aligned}\mathcal{G}_{HH}|^{\text{close}}_{\text{right}} = &-\frac{1}{4\pi}\ln\left[4\,\mathrm{sh}\left(\frac{\lambda}{2}(x-x'-t)\right)\mathrm{sh}\left(\frac{\lambda}{2}(x-x'+t)\right)+i\epsilon\right]\\ &+\frac{\lambda}{4\pi m}+\frac{\lambda}{4\pi m}\cdot\frac{m-q\lambda}{m+q\lambda}\mathrm{e}^{-m(x+x')}\,.\end{aligned} \tag{C.12}$$

This expression is valid under eq. (C.10), together with $m|x-x'|, m|t| \ll 1$, $|t| < x+x'$. In the limit $q \to 0$ it reduces to the expression found in [41].

Unruh Green's function (left):

$$\begin{aligned}\mathcal{G}_U|^{\text{close}}_{\text{left}} = &-\frac{1}{4\pi}\ln\left[2\,\mathrm{sh}\left(\frac{\lambda}{2}(x-x'-t)\right)m(x-x'+t)+i\epsilon\right]-\frac{\lambda(x+x')}{4\pi}\\ &+\frac{\lambda}{2\pi^2 m}\mathcal{H}\left(\frac{q\lambda}{m}\right)+\frac{1}{8\pi}\mathcal{H}^{(1)}\left(\frac{q\lambda}{m}\right)\,,\end{aligned} \tag{C.13}$$

where

$$\mathcal{H}(y) = -\frac{1}{y^2}-\frac{(1+y^2)^2\,\mathrm{arctg}\,y}{y^3(y^2-1)}+\frac{\pi y}{y^2-1}\,, \tag{C.14a}$$

$$\mathcal{H}^{(1)}(y) = \frac{1}{y^2}-\frac{(1+y^2)^2\ln[1+y^2]}{y^4}+2(\ln 2-\gamma_E)\,. \tag{C.14b}$$

This formula is valid under the conditions (C.9), $|x - x' + t| \ll \min\{m^{-1}, (q\lambda)^{-1}\}$, and $|t| < |x + x'|$.

The functions $\mathcal{H}$, $\mathcal{H}^{(1)}$ are regular in the limit $y \to 0$:

$$\mathcal{H}(0) = \frac{8}{3} , \quad \mathcal{H}^{(1)}(0) = -\frac{3}{2} + 2(\ln 2 - \gamma_E) , \tag{C.15}$$

which corresponds to vanishing barrier, and the function $\mathcal{G}_U|^{\text{close}}_{\text{left}}$ reduces to that derived in [41]. In the opposite limit $y \to \infty$ the asymptotics of $\mathcal{H}$, $\mathcal{H}^{(1)}$ are

$$\mathcal{H}(y) \approx \frac{\pi}{2y} , \quad \mathcal{H}^{(1)}(y) \approx -2(\ln y - \ln 2 + \gamma_E) , \quad y \to \infty . \tag{C.16}$$

The function $\mathcal{H}(y)$ is monotonic, it is plotted in Fig. 14.

Unruh Green's function (right):

$$\mathcal{G}_U|^{\text{close}}_{\text{right}} = \mathcal{G}_U|^{\text{close}}_{\text{far}} + \Delta\mathcal{G}_U , \tag{C.17}$$

where

$$\begin{aligned} \mathcal{G}_U|^{\text{close}}_{\text{far}} = &- \frac{1}{4\pi} \ln \left[2 \operatorname{sh} \left(\frac{\lambda}{2}(x - x' - t) \right) m(x - x' + t) + i\epsilon \right] \\ &+ \frac{\lambda}{2\pi^2 m} \tilde{\mathcal{H}} \left(\frac{q\lambda}{m} \right) + \frac{1}{8\pi} \tilde{\mathcal{H}}^{(1)} \left(\frac{q\lambda}{m} \right) , \end{aligned} \tag{C.18}$$

and

$$\Delta\mathcal{G}_U = \begin{cases} \frac{\lambda}{2\pi^2 m} \left[\mathcal{H}\left(\frac{q\lambda}{m}\right) - \tilde{\mathcal{H}}\left(\frac{q\lambda}{m}\right) \right] + \frac{\lambda(x+x')}{4\pi} \left[\frac{2q\lambda}{\pi m} \mathcal{H}\left(\frac{q\lambda}{m}\right) - 1 \right] + \frac{1}{8\pi} \tilde{\mathcal{H}}^{(2)}\left(\frac{q\lambda}{m}\right) , & x+x' \ll \min\{\frac{1}{q\lambda}, \frac{1}{m}\} \\ \frac{1}{2\pi} \ln[m(x + x')] - \frac{\ln 2 - \gamma_E}{2\pi}, & \frac{1}{q\lambda} \ll x+x' \ll \frac{1}{m} \\ 0, & \frac{1}{m} \ll x+x' \end{cases} \tag{C.19}$$

Here

$$\tilde{\mathcal{H}}(y) = -\frac{1}{y^2} + \frac{(1 + y^2) \operatorname{arctg} y}{y^3} , \tag{C.20a}$$

$$\tilde{\mathcal{H}}^{(1)}(y) = \frac{1}{y^2} + \frac{(y^4 - 1) \ln(1 + y^2)}{y^4} + 2(\ln 2 - \gamma_E) , \tag{C.20b}$$

$$\tilde{\mathcal{H}}^{(2)}(y) = -\frac{2(1 + y^2)}{y^2} \ln(1 + y^2) . \tag{C.20c}$$

Note that the intermediate range in (C.19) exists only if $m \ll q\lambda$. In all above expressions we assume eq. (C.10), $|x - x' - t| \ll \min\{m^{-1}, (q\lambda)^{-1}\}$, $|x - x' + t| \ll m^{-1}$ and $|t| < x + x'$.

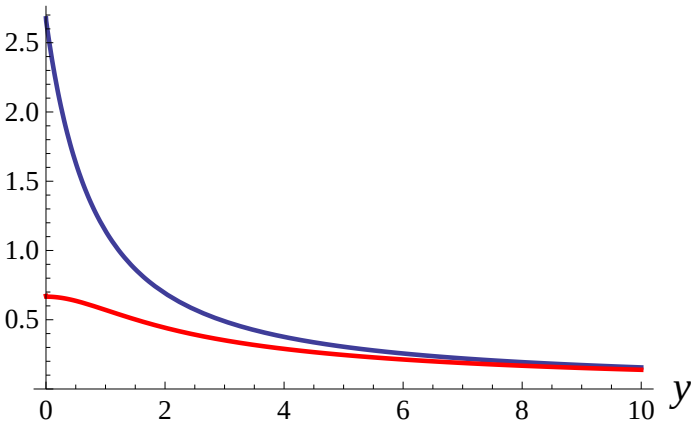


Figure 14: Functions $\mathcal{H}(y)$ (blue) and $\tilde{\mathcal{H}}(y)$ (red) given by eqs. (C.14a) and (C.20a).

In the limit of vanishing barrier, $y \to 0$, the functions $\tilde{\mathcal{H}}$, $\tilde{\mathcal{H}}^{(1)}$, $\tilde{\mathcal{H}}^{(2)}$ reduce to

$$\tilde{\mathcal{H}}(0) = \frac{2}{3}\,, \quad \tilde{\mathcal{H}}^{(1)}(0) = \frac{1}{2} + 2(\gamma_E - \ln 2)\,, \quad \tilde{\mathcal{H}}^{(2)}(0) = -2\,, \tag{C.21}$$

and the expression for $\mathcal{G}_U|^{\text{close}}_{\text{right}}$ derived in [41] is reproduced. In the opposite limit $y \to \infty$ the asymptotics of $\tilde{\mathcal{H}}$, $\tilde{\mathcal{H}}^{(1)}$, $\tilde{\mathcal{H}}^{(2)}$ are

$$\tilde{\mathcal{H}}(y) \approx \frac{\pi}{2y}\,, \quad \tilde{\mathcal{H}}^{(1)}(y) \approx 2(\ln y + \ln 2 - \gamma_E)\,, \quad \tilde{\mathcal{H}}^{(2)}(y) \approx -4\ln y\,, \quad y \to \infty\,. \tag{C.22}$$

The function $\tilde{\mathcal{H}}(y)$ is monotonic and is plotted in Fig. 14.

C.3 Calculation of the Green's functions

Hartle–Hawking Green's function (left). We start from the general expression for the Green's function in terms of the reflection amplitude [41],

$$\mathcal{G}_{HH}|_{\text{left}} = \int_0^\infty \frac{\mathrm{d}\omega}{4\pi\omega}\left[2\cos\omega(x-x') + \beta_\omega \mathrm{e}^{-i\omega(x+x')} + \beta_\omega^* \mathrm{e}^{i\omega(x+x')}\right] S(\omega)\,, \tag{C.23}$$

where

$$S(\omega) = \frac{\mathrm{e}^{-i\omega|t|}}{1-\mathrm{e}^{-\frac{2\pi\omega}{\lambda}}} + \frac{\mathrm{e}^{i\omega|t|}}{\mathrm{e}^{\frac{2\pi\omega}{\lambda}}-1}\,. \tag{C.24}$$

Let us split the domain of integration in two parts $0 \le \omega < m$ and $m \le \omega < \infty$ and write

$$\mathcal{G}_{HH}|_{\text{left}} = \mathcal{G}^{(1)}_{HH} + \mathcal{G}^{(2)}_{HH}\,, \tag{C.25}$$

where the integration in the two terms runs over the first and second domain, respectively. We first evaluate $\mathcal{G}^{(2)}_{HH}$. Using the identities $S(-\omega) = -S(\omega)$, $\beta^*_\omega = \beta_{-\omega}$, it can be brought to the form

$$\mathcal{G}^{(2)}_{HH} = \int_{\mathscr{B}} \frac{\mathrm{d}\omega}{4\pi\omega}\left[\mathrm{e}^{i\omega(x-x')} + \beta_\omega \mathrm{e}^{-i\omega(x+x')}\right] S(\omega)\,, \tag{C.26}$$

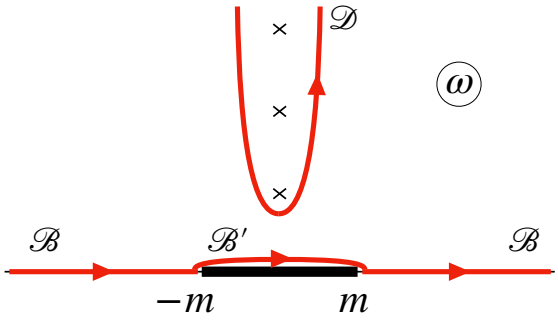


Figure 15: Contours in the ω-plane used in the calculation of the Hartle–Hawking Green's function and of the Unruh Green's function at $q\lambda < m$.

where $\mathscr{B} = (-\infty, -m] \cup [m, \infty)$, see Fig. 15. To this we add and subtract the integral over $\mathscr{B}'$ — the upper side of the branch cut at $-m < \omega < m$. If $x - x' > |t|$ and $|x + x'| > |t|$, the contour $\mathscr{B} \cup \mathscr{B}'$ can be deformed into the contour $\mathscr{D}$ that encircles the poles of $S(\omega)$ at $\omega = i\lambda n$, $n = 1, 2, \ldots$ as shown in Fig. 15.[14] Since $m \ll \lambda$ and $q \ll 1$, we can set $\beta_\omega = 0$ when computing the residues over these poles. We obtain

$$\begin{aligned} \mathcal{G}^{(2)}_{HH} = &- \frac{1}{4\pi} \ln \left[1 - 2\mathrm{e}^{-\lambda(x-x')} \operatorname{ch} \lambda t + \mathrm{e}^{-2\lambda(x-x')}\right] \\ &- \int_{-m+i\epsilon}^{m+i\epsilon} \frac{\mathrm{d}\omega}{4\pi\omega} \left[\mathrm{e}^{i\omega(x-x')} + \beta_\omega \mathrm{e}^{-i\omega(x+x')}\right] S(\omega) \,. \end{aligned} \tag{C.27}$$

We now turn to $\mathcal{G}^{(1)}_{HH}$. This can be written as

$$\mathcal{G}^{(1)}_{HH} = \fint_{-m}^{m} \frac{\mathrm{d}\omega}{4\pi\omega} \left[\mathrm{e}^{i\omega(x-x')} + \beta_\omega \mathrm{e}^{-i\omega(x+x')}\right] S(\omega) \,, \tag{C.28}$$

where the integral is understood in the sense of principal value. We observe that this almost cancels with the second term in (C.27), up to a half-residue at the origin. The difference equals to $-\lambda x/(2\pi) + \lambda/(2\pi(m + q\lambda))$. We combine it with the first line of eq. (C.27) and analytically continue to $x - x' < |t|$ to obtain eq. (C.11).

Hartle–Hawking Green's function (right). Here the general expression is [41]

$$\begin{aligned} \mathcal{G}_{HH}|_{\text{right}} = &\int_m^\infty \frac{\mathrm{d}\omega}{4\pi k} \left[2\cos k(x-x') - \frac{\gamma^*_\omega \beta_\omega}{\gamma_\omega} \mathrm{e}^{-ik(x+x')} - \frac{\gamma_\omega \beta^*_\omega}{\gamma^*_\omega} \mathrm{e}^{ik(x+x')}\right] S(\omega) \\ &+ \int_0^m \frac{\mathrm{d}\omega}{4\pi\omega} |\gamma_\omega|^2 \mathrm{e}^{-\varkappa(x+x')} S(\omega) \,, \end{aligned} \tag{C.29}$$

[14] Note that β_ω does not have singularities in the upper half-plane due to the absence of bound states in the potential (2.11).

where k and $\varkappa$ are given by eqs. (C.4), (C.6). Note that the last term describes contribution of the non-propagating modes localized on the BH. We can manipulate the integrals in the same way as in the previous paragraph. The only new twist are the restrictions on $|x-x'|$, $|t|$ that must be fulfilled to bring the result to the final form eq. (C.12). We leave the details of the derivation to the reader.

Unruh Green's function (left). Our starting point is the relation between the Unruh and Hartle–Hawking Green's functions in the left region [41],

$$\mathcal{G}_U|_{\text{left}} = \mathcal{G}_{HH}|_{\text{left}} - \int_m^\infty \frac{\mathrm{d}\omega\, k}{2\pi\omega^2}\,|\gamma_\omega|^2\,\frac{\cos[\omega(x-x'+t)]}{\mathrm{e}^{2\pi\omega/\lambda}-1}\ . \tag{C.30}$$

Let us evaluate the second term which we denote by $\mathcal{G}_U^{(2)}$. Viewing $k(\omega)$ and $|\gamma_\omega|^2$ as analytic functions of ω in the upper half-plane and using $k(-\omega)=-k(\omega)$, $|\gamma_{-\omega}|^2=|\gamma_\omega|^2$ for $\omega>m$, we can bring it to the form

$$\mathcal{G}_U^{(2)} = -\int_{\mathscr{B}} \frac{\mathrm{d}\omega\, k}{4\pi\omega^2}|\gamma_\omega|^2\frac{\mathrm{e}^{i\omega(x-x'+t)}}{1-\mathrm{e}^{-\frac{2\pi\omega}{\lambda}}} + \int_m^\infty \frac{\mathrm{d}\omega\, k}{4\pi\omega^2}|\gamma_\omega|^2\mathrm{e}^{i\omega(x-x'+t)}\ , \tag{C.31}$$

where $\mathscr{B}=(\infty,-m]\cup[m,\infty)$. Now we add and subtract the integral over $\mathscr{B}'$—the upper side of the branch cut at $-m<\omega<m$. Let us assume that $x-x'+t>0$ (we will analytically continue to negative $x-x'+t$ at the end). Then the contour $\mathscr{B}\cup\mathscr{B}'$ can be deformed into the upper half-plane. This deformation picks up the thermal poles at $\omega=in\lambda$, $n=1,2,...$, as in the case of the Hartle–Hawking Green's function, see Fig. 15.

In addition, we should consider the singularities of the transmission coefficient $|\gamma_\omega|^2$. Using eq. (C.7b), we see that for $q\lambda<m$ it does not have any poles in the upper half-plane. On the other hand, for $q\lambda>m$ a single pole appears at

$$\omega_q = \frac{i}{2q\lambda}((q\lambda)^2-m^2)\ . \tag{C.32}$$

Since $q\ll 1$, this pole always stays well below the first thermal pole at $\omega=i\lambda$, see Fig. 16.

All in all we write,

$$\mathcal{G}_U^{(2)} = \mathcal{G}_U^{(21)} + \mathcal{G}_U^{(22)} + \mathcal{G}_U^{(23)} + \mathcal{G}_U^{(24)}\ , \tag{C.33}$$

where the first three terms stand for the integrals along the contours $\mathscr{D}$, $-\mathscr{B}'$ and $\mathscr{D}'$ shown in Fig. 16, whereas $\mathcal{G}_U^{(24)}$ is just the second term in eq. (C.31). Let us evaluate these four contributions one by one.

Since $m\ll\lambda$ and $q\ll 1$, we can set $|\gamma_\omega|^2=1$ in $\mathcal{G}_U^{(21)}$, and the result is

$$\mathcal{G}_U^{(21)} = \frac{1}{4\pi}\ln\left[1-\mathrm{e}^{-\lambda(x-x'+t)}\right]\ . \tag{C.34}$$

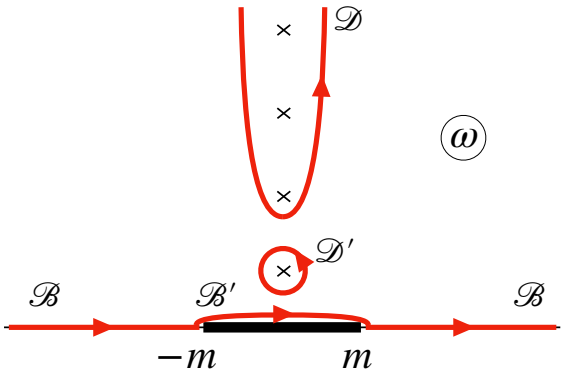


Figure 16: Contours in the ω-plane used in the calculation of the Unruh Green's function at $q\lambda > m$.

In $\mathcal{G}_U^{(22)}$ we use eq. (C.7b) at $\omega < m$, assume $m(x-x'+t) \ll 1$ and expand the integrand to the subleading orders in ω/λ and $\omega(x-x'+t)$ to retain $\mathcal{O}(1)$-contributions. We obtain

$$\mathcal{G}_U^{(22)} = \frac{i\lambda}{2\pi^2}\int_{-m+i\epsilon}^{m+i\epsilon} \frac{\mathrm{d}\omega\,\varkappa}{\omega((\omega+i\varkappa)^2+(q\lambda)^2)} + \left(\frac{i}{2\pi} - \frac{\lambda(x-x'+t)}{2\pi^2}\right)\int_{-m}^{m}\frac{\mathrm{d}\omega\,\varkappa}{(\omega+i\varkappa)^2+(q\lambda)^2}\,. \tag{C.35}$$

Evaluating the integrals, we arrive at

$$\begin{aligned}\mathcal{G}_U^{(22)} = &-\frac{\lambda}{4\pi^2 m}\left\{\frac{2}{y^2} + \frac{(1+y^2)^2\,\mathrm{arctg}\left(\frac{2y}{1-y^2}\right)}{y^3(y^2-1)} - \frac{2\pi}{y^2-1}\right\} \\ &+\left(-\frac{i}{8}+\frac{\lambda(x-x'+t)}{8\pi}\right)\left(\theta(1-y) - \frac{1+2y^2}{4y^4}\theta(y-1)\right)\,,\end{aligned} \tag{C.36}$$

where we have denoted

$$y = \frac{q\lambda}{m} \tag{C.37}$$

and $\theta(x)$ is the Heaviside step-function.

In $\mathcal{G}_U^{(23)}$ we assume again that $m(x-x'+t) \ll 1$ and, moreover, $q\lambda(x-x'+t) \ll 1$. Evaluation of the residue at $\omega = \omega_q$ yields

$$\mathcal{G}_U^{(23)} = \left[-\frac{\lambda}{4\pi m}\frac{(1+y^2)^2}{y^3(y^2-1)} + \left(-\frac{i}{8}+\frac{\lambda(x-x'+t)}{8\pi}\right)\frac{(1+y^2)^2}{y^4}\right]\theta(y-1)\,. \tag{C.38}$$

In $\mathcal{G}_U^{(24)}$ we assume that both $m(x-x'+t) \ll 1$ and $q\lambda(x-x'+t) \ll 1$ and split the integration domain into $[m,\omega_*)$ and $[\omega_*,\infty)$ where $m, q\lambda \ll \omega_* \ll |x-x'+t|^{-1}$. We then approximate the exponent $\mathrm{e}^{i\omega(x-x'+t)}$ by 1 in the first sub-integral and approximate the

transmission coefficient by 1 in the second sub-integral. In this way we get

$$\mathcal{G}_U^{(24)} = -\frac{1}{4\pi}\ln\left[m(x-x'+t)\right] + \frac{\ln 2-\gamma_E}{4\pi} + \frac{i}{8} + \frac{y^2-(1+y^2)^2\ln[1+y^2]}{8\pi y^4}\,. \tag{C.39}$$

Finally, we combine all four terms together and use the identity

$$\operatorname{arctg}\left(\frac{2y}{1-y^2}\right) + \pi\theta(y-1) = 2\operatorname{arctg} y\,. \tag{C.40}$$

Note that, despite the presence of discontinuities at $y=1$ in the individual terms of eq. (C.33), the sum is continuous and smooth at this point. The discontinuity coming with the pole at $\omega=\omega_q$ (eq. (C.32)) that appears in the upper half-plane at $y>1$ is exactly canceled by the discontinuity in the term $\mathcal{G}_U^{(22)}$.

It remains to perform analytic continuation to $x-x'+t<0$ and add the result to the Hartle–Hawking Green's function $\mathcal{G}_{HH}|_{\text{left}}$. This leads to eq. (C.13).

Unruh Green's function (right). The Unruh Green's function in the right region is related to the Hartle–Hawking one as follows

$$\begin{aligned}\mathcal{G}_U|_{\text{right}} = \mathcal{G}_{HH}|_{\text{right}} &- \int_m^\infty \frac{\mathrm{d}\omega}{2\pi k}\,\frac{\cos[k(x-x')+\omega t)] + |\beta_\omega|^2\cos[k(x-x')-\omega t)]}{\mathrm{e}^{2\pi\omega/\lambda}-1} \\ &+ \int_m^\infty \frac{\mathrm{d}\omega}{2\pi k}\left[\frac{\gamma_\omega^*\beta_\omega}{\gamma_\omega}\mathrm{e}^{-ik(x+x')} + \frac{\gamma_\omega\beta_\omega^*}{\gamma_\omega^*}\mathrm{e}^{ik(x+x')}\right]\frac{\cos\omega t}{\mathrm{e}^{2\pi\omega/\lambda}-1}\,.\end{aligned} \tag{C.41}$$

The second term here, which we denote by $\tilde{\mathcal{G}}_U^{(2)}$, is computed following the same steps as in the previous paragraph. We do not present them in detail and just quote the result,

$$\begin{aligned}\tilde{\mathcal{G}}_U^{(2)} =& \frac{1}{4\pi}\ln\left[\frac{2\operatorname{sh}\frac{\lambda}{2}(x-x'+t)}{m(x-x'+t)}\right] + \frac{\lambda}{2\pi^2 m}\left\{-\frac{1}{y^2}+\frac{1+y^2}{y^3}\operatorname{arctg} y - \frac{\pi}{2}\right\} \\ &+ \frac{1}{8\pi}\left[\frac{1}{y^2}+\frac{y^4-1}{y^4}\ln(1+y^2) + 2(\ln 2-\gamma_E)\right],\end{aligned} \tag{C.42}$$

where y is defined in eq. (C.37). In deriving this expression we have assumed $m|x-x'+t|\ll 1$, $m|x-x'-t|\ll 1$ and $q\lambda|x-x'-t|\ll 1$. Combining this with the Hartle–Hawking Green's function (C.12) far away from the BH, we obtain the result (C.18).

The third term in eq. (C.41) is localized in the vicinity of the BH. Let us denote it by $\tilde{\mathcal{G}}_U^{(3)}$. Substituting the expressions (C.7) for the reflection and transmission amplitudes we obtain,

$$\tilde{\mathcal{G}}_U^{(3)} = \int_m^\infty \frac{\mathrm{d}\omega}{2\pi k}\left[\frac{i(\omega-k)+q\lambda}{i(\omega+k)+q\lambda}\mathrm{e}^{-ik(x+x')} + \text{h.c.}\right]\frac{\cos\omega t}{\mathrm{e}^{2\pi\omega/\lambda}-1}\,. \tag{C.43}$$

We observe that the integral converges at $\omega \lesssim \max\{m, q\lambda\} \ll \lambda$. Thus, we can expand the thermal factor up to the first subleading term to keep track of $\mathcal{O}(1)$ contributions. If we

further assume $|t| < x + x' \ll \min\{m^{-1}, (q\lambda)^{-1}\}$, we can also expand the exponential factor $\mathrm{e}^{-ik(x+x')}$ and replace $\cos\omega t$ with 1. Then the integrals are easily taken and we get

$$\tilde{\mathcal{G}}_U^{(3)} = \frac{\lambda}{2\pi^2 m}\left[\frac{\pi(y^2+1)}{2(y^2-1)} - \frac{2(1+y^2)}{y(y^2-1)}\operatorname{arctg} y\right] - \frac{(1+y^2)\ln(1+y^2)}{4\pi y^2} + \frac{\lambda(x+x')}{4\pi}\left[-\frac{2}{\pi y} + \frac{2y}{y^2-1} - \frac{2(1+y^2)^2}{\pi y^2(y^2-1)}\operatorname{arctg} y\right], \qquad |t| < x + x' \ll \min\{\tfrac{1}{m}, \tfrac{1}{q\lambda}\}. \tag{C.44}$$

If, on the other hand, $x + x' \gg m^{-1}$, the integrand is quickly oscillating and the integral is damped, so we obtain

$$\tilde{\mathcal{G}}_U^{(3)} \approx 0, \qquad x + x' \gg \tfrac{1}{m}. \tag{C.45}$$

The intermediate range $(q\lambda)^{-1} \ll x+x' \ll m^{-1}$, which exists only for very high temperatures, requires a careful examination of various contributions. We leave this exercise to the reader. The result is

$$\tilde{\mathcal{G}}_U^{(3)} = \frac{\lambda}{2\pi^2 m}\left(\frac{\pi}{2} - \frac{\pi}{y}\right) + \frac{\lambda(x+x')}{4\pi}\left(-1 + \frac{2}{y}\right) + \frac{1}{2\pi}\ln[m(x+x')] - \frac{\ln 2 - \gamma_E}{2\pi}, \quad \tfrac{1}{q\lambda} \ll x+x' \ll \tfrac{1}{m}. \tag{C.46}$$

Combining these expressions with the Hartle–Hawking Green's function (C.12) in the BH vicinity, we arrive at eq. (C.19).

References

[1] W. A. Hiscock, "Can black holes nucleate vacuum phase transitions?," *Phys. Rev.* **D35** (1987) 1161–1170.

[2] V. A. Berezin, V. A. Kuzmin, and I. I. Tkachev, "O(3) Invariant Tunneling in General Relativity," *Phys. Lett.* **B207** (1988) 397–403.

[3] P. B. Arnold, "Gravity and false vacuum decay rates: O(3) solutions," *Nucl. Phys.* **B346** (1990) 160–192.

[4] V. A. Berezin, V. A. Kuzmin, and I. I. Tkachev, "Black holes initiate false vacuum decay," *Phys. Rev.* **D43** (1991) 3112–3116.

[5] R. Gregory, I. G. Moss, and B. Withers, "Black holes as bubble nucleation sites," *JHEP* **03** (2014) 081, arXiv:1401.0017 [hep-th].

[6] P. Burda, R. Gregory, and I. Moss, "Gravity and the stability of the Higgs vacuum," *Phys. Rev. Lett.* **115** (2015) 071303, arXiv:1501.04937 [hep-th].

[7] P. Burda, R. Gregory, and I. Moss, "Vacuum metastability with black holes," *JHEP* **08** (2015) 114, arXiv:1503.07331 [hep-th].

[8] P. Burda, R. Gregory, and I. Moss, "The fate of the Higgs vacuum," *JHEP* **06** (2016) 025, arXiv:1601.02152 [hep-th].

[9] N. Tetradis, "Black holes and Higgs stability," *JCAP* **1609** no. 09, (2016) 036, arXiv:1606.04018 [hep-ph].

[10] D. Canko, I. Gialamas, G. Jelic-Cizmek, A. Riotto, and N. Tetradis, "On the Catalysis of the Electroweak Vacuum Decay by Black Holes at High Temperature," *Eur. Phys. J.* **C78** no. 4, (2018) 328, arXiv:1706.01364 [hep-th].

[11] D. Gorbunov, D. Levkov, and A. Panin, "Fatal youth of the Universe: black hole threat for the electroweak vacuum during preheating," *JCAP* **1710** no. 10, (2017) 016, arXiv:1704.05399 [astro-ph.CO].

[12] K. Mukaida and M. Yamada, "False Vacuum Decay Catalyzed by Black Holes," *Phys. Rev.* **D96** no. 10, (2017) 103514, arXiv:1706.04523 [hep-th].

[13] K. Kohri and H. Matsui, "Electroweak Vacuum Collapse induced by Vacuum Fluctuations of the Higgs Field around Evaporating Black Holes," *Phys. Rev.* **D98** no. 12, (2018) 123509, arXiv:1708.02138 [hep-ph].

[14] D.-C. Dai, R. Gregory, and D. Stojkovic, "Connecting the Higgs Potential and Primordial Black Holes," *Phys. Rev. D* **101** no. 12, (2020) 125012, arXiv:1909.00773 [hep-ph].

[15] T. Hayashi, K. Kamada, N. Oshita, and J. Yokoyama, "On catalyzed vacuum decay around a radiating black hole and the crisis of the electroweak vacuum," *JHEP* **08** (2020) 088, arXiv:2005.12808 [hep-th].

[16] T. Miyachi and J. Soda, "False vacuum decay in a two-dimensional black hole spacetime," *Phys. Rev. D* **103** no. 8, (2021) 085009, arXiv:2102.02462 [gr-qc].

[17] R. A. Flores and M. Sher, "Upper Limits to Fermion Masses in the Glashow-Weinberg-Salam Model," *Phys. Rev. D* **27** (1983) 1679.

[18] M. Sher, "Electroweak Higgs Potentials and Vacuum Stability," *Phys. Rept.* **179** (1989) 273–418.

[19] G. Isidori, G. Ridolfi, and A. Strumia, "On the metastability of the standard model vacuum," *Nucl. Phys. B* **609** (2001) 387–409, arXiv:hep-ph/0104016.

[20] F. Bezrukov, M. Yu. Kalmykov, B. A. Kniehl, and M. Shaposhnikov, "Higgs Boson Mass and New Physics," *JHEP* **10** (2012) 140, arXiv:1205.2893 [hep-ph].

[21] G. Degrassi, S. Di Vita, J. Elias-Miro, J. R. Espinosa, G. F. Giudice, G. Isidori, and A. Strumia, "Higgs mass and vacuum stability in the Standard Model at NNLO," *JHEP* **08** (2012) 098, arXiv:1205.6497 [hep-ph].

[22] D. Buttazzo, G. Degrassi, P. P. Giardino, G. F. Giudice, F. Sala, A. Salvio, and A. Strumia, "Investigating the near-criticality of the Higgs boson," *JHEP* **12** (2013) 089, arXiv:1307.3536 [hep-ph].

[23] A. V. Bednyakov, B. A. Kniehl, A. F. Pikelner, and O. L. Veretin, "Stability of the Electroweak Vacuum: Gauge Independence and Advanced Precision," *Phys. Rev. Lett.* **115** no. 20, (2015) 201802, arXiv:1507.08833 [hep-ph].

[24] T. Markkanen, A. Rajantie, and S. Stopyra, "Cosmological Aspects of Higgs Vacuum Metastability," *Front. Astron. Space Sci.* **5** (2018) 40, arXiv:1809.06923 [astro-ph.CO].

[25] S. R. Coleman, "The Fate of the False Vacuum. 1. Semiclassical Theory," *Phys. Rev.* **D15** (1977) 2929–2936. [Erratum: Phys. Rev.D16,1248(1977)].

[26] C. G. Callan, Jr. and S. R. Coleman, "The Fate of the False Vacuum. 2. First Quantum Corrections," *Phys. Rev.* **D16** (1977) 1762–1768.

[27] S. R. Coleman, "The Uses of Instantons," *Subnucl. Ser.* **15** (1979) 805.

[28] S. R. Coleman and F. De Luccia, "Gravitational Effects on and of Vacuum Decay," *Phys. Rev.* **D21** (1980) 3305.

[29] J. B. Hartle and S. W. Hawking, "Path Integral Derivation of Black Hole Radiance," *Phys. Rev.* **D13** (1976) 2188–2203.

[30] J. Garcia-Bellido, A. D. Linde, and D. Wands, "Density perturbations and black hole formation in hybrid inflation," *Phys. Rev. D* **54** (1996) 6040–6058, arXiv:astro-ph/9605094.

[31] T. Fujita, M. Kawasaki, K. Harigaya, and R. Matsuda, "Baryon asymmetry, dark matter, and density perturbation from primordial black holes," *Phys. Rev. D* **89** no. 10, (2014) 103501, arXiv:1401.1909 [astro-ph.CO].

[32] R. Dong, W. H. Kinney, and D. Stojkovic, "Gravitational wave production by Hawking radiation from rotating primordial black holes," *JCAP* **10** (2016) 034, arXiv:1511.05642 [astro-ph.CO].

[33] R. Allahverdi, J. Dent, and J. Osinski, "Nonthermal production of dark matter from primordial black holes," *Phys. Rev. D* **97** no. 5, (2018) 055013, arXiv:1711.10511 [astro-ph.CO].

[34] O. Lennon, J. March-Russell, R. Petrossian-Byrne, and H. Tillim, "Black Hole Genesis of Dark Matter," *JCAP* **04** (2018) 009, arXiv:1712.07664 [hep-ph].

[35] L. Morrison, S. Profumo, and Y. Yu, "Melanopogenesis: Dark Matter of (almost) any Mass and Baryonic Matter from the Evaporation of Primordial Black Holes weighing a Ton (or less)," *JCAP* **05** (2019) 005, arXiv:1812.10606 [astro-ph.CO].

[36] D. Hooper, G. Krnjaic, and S. D. McDermott, "Dark Radiation and Superheavy Dark Matter from Black Hole Domination," *JHEP* **08** (2019) 001, arXiv:1905.01301 [hep-ph].

[37] B. Carr, K. Kohri, Y. Sendouda, and J. Yokoyama, "Constraints on Primordial Black Holes," arXiv:2002.12778 [astro-ph.CO].

[38] D. Hooper, G. Krnjaic, J. March-Russell, S. D. McDermott, and R. Petrossian-Byrne, "Hot Gravitons and Gravitational Waves From Kerr Black Holes in the Early Universe," arXiv:2004.00618 [astro-ph.CO].

[39] **Particle Data Group** Collaboration, P. A. Zyla *et al.*, "Review of Particle Physics," *PTEP* **2020** no. 8, (2020) 083C01.

[40] W. G. Unruh, "Notes on black hole evaporation," *Phys. Rev.* **D14** (1976) 870.

[41] A. Shkerin and S. Sibiryakov, "Black hole induced false vacuum decay from first principles," arXiv:2105.09331 [hep-th].

[42] W. H. Miller, "Classical-limit quantum mechanics and the theory of molecular collisions," in *Advances in Chemical Physics*, pp. 69–177. John Wiley & Sons, Ltd, 1974. https://onlinelibrary.wiley.com/doi/abs/10.1002/9780470143773.ch2.

[43] V. A. Rubakov, D. T. Son, and P. G. Tinyakov, "Classical boundary value problem for instanton transitions at high-energies," *Phys. Lett. B* **287** (1992) 342–348.

[44] G. F. Bonini, A. G. Cohen, C. Rebbi, and V. A. Rubakov, "The Semiclassical description of tunneling in scattering with multiple degrees of freedom," *Phys. Rev. D* **60** (1999) 076004, arXiv:hep-ph/9901226.

[45] F. L. Bezrukov and D. Levkov, "Dynamical tunneling of bound systems through a potential barrier: complex way to the top," *J. Exp. Theor. Phys.* **98** (2004) 820–836, arXiv:quant-ph/0312144.

[46] S. F. Bramberger, G. Lavrelashvili, and J.-L. Lehners, "Quantum tunneling from paths in complex time," *Phys. Rev. D* **94** no. 6, (2016) 064032, arXiv:1605.02751 [hep-th].

[47] N. Turok, "On Quantum Tunneling in Real Time," *New J. Phys.* **16** (2014) 063006, arXiv:1312.1772 [quant-ph].

[48] A. Cherman and M. Unsal, "Real-Time Feynman Path Integral Realization of Instantons," arXiv:1408.0012 [hep-th].

[49] A. D. Plascencia and C. Tamarit, "Convexity, gauge-dependence and tunneling rates," *JHEP* **10** (2016) 099, arXiv:1510.07613 [hep-ph].

[50] A. Andreassen, D. Farhi, W. Frost, and M. D. Schwartz, "Direct Approach to Quantum Tunneling," *Phys. Rev. Lett.* **117** no. 23, (2016) 231601, arXiv:1602.01102 [hep-th].

[51] A. Andreassen, D. Farhi, W. Frost, and M. D. Schwartz, "Precision decay rate calculations in quantum field theory," *Phys. Rev.* **D95** no. 8, (2017) 085011, arXiv:1604.06090 [hep-th].

[52] M. C. Johnson, *private communication*.

[53] C. G. Callan, Jr., S. B. Giddings, J. A. Harvey, and A. Strominger, "Evanescent black holes," *Phys. Rev.* **D45** no. 4, (1992) R1005, arXiv:hep-th/9111056 [hep-th].

[54] N. D. Birrell and P. C. W. Davies, *Quantum Fields in Curved Space*. Cambridge Monographs on Mathematical Physics. Cambridge Univ. Press, Cambridge, UK, 1984.

[55] S. R. Coleman, V. Glaser, and A. Martin, "Action Minima Among Solutions to a Class of Euclidean Scalar Field Equations," *Commun. Math. Phys.* **58** (1978) 211–221.

[56] K. Blum, M. Honda, R. Sato, M. Takimoto, and K. Tobioka, "O(N) Invariance of the Multi-Field Bounce," *JHEP* **05** (2017) 109, arXiv:1611.04570 [hep-th]. [Erratum: JHEP06,060(2017)].

[57] J. Byeon, L. Jeanjean, and M. Mariş, "Symmetry and monotonicity of least energy solutions," *arXiv e-prints* (June, 2008) , arXiv:0806.0299 [math.AP].

[58] A. D. Linde, "Decay of the False Vacuum at Finite Temperature," *Nucl. Phys. B* **216** (1983) 421. [Erratum: Nucl.Phys.B 223, 544 (1983)].

[59] A. D. Linde, "Fate of the False Vacuum at Finite Temperature: Theory and Applications," *Phys. Lett.* **100B** (1981) 37–40.

[60] W.-Y. Ai, "Correspondence between Thermal and Quantum Vacuum Transitions around Horizons," *JHEP* **03** (2019) 164, arXiv:1812.06962 [hep-th].

[61] V. Briaud, A. Shkerin, and S. Sibiryakov, *in preparation*.

[62] D. Y. Grigoriev and V. A. Rubakov, "Soliton Pair Creation at Finite Temperatures. Numerical Study in (1+1)-dimensions," *Nucl. Phys. B* **299** (1988) 67–78.

[63] D. Y. Grigoriev, V. A. Rubakov, and M. E. Shaposhnikov, "Sphaleron Transitions at Finite Temperatures: Numerical Study in (1+1)-dimensions," *Phys. Lett. B* **216** (1989) 172–176.

[64] D. Y. Grigoriev, V. A. Rubakov, and M. E. Shaposhnikov, "Topological transitions at finite temperatures: a real time numerical approach," *Nucl. Phys. B* **326** (1989) 737–757.

[65] S. Khlebnikov, L. Kofman, A. D. Linde, and I. Tkachev, "First order nonthermal phase transition after preheating," *Phys. Rev. Lett.* **81** (1998) 2012–2015, arXiv:hep-ph/9804425.

[66] J. Braden, M. C. Johnson, H. V. Peiris, A. Pontzen, and S. Weinfurtner, "New Semiclassical Picture of Vacuum Decay," *Phys. Rev. Lett.* **123** no. 3, (2019) 031601, arXiv:1806.06069 [hep-th].

[67] M. P. Hertzberg and M. Yamada, "Vacuum Decay in Real Time and Imaginary Time Formalisms," *Phys. Rev. D* **100** no. 1, (2019) 016011, arXiv:1904.08565 [hep-th].

[68] M. P. Hertzberg, F. Rompineve, and N. Shah, "Quantitative Analysis of the Stochastic Approach to Quantum Tunneling," *Phys. Rev. D* **102** no. 7, (2020) 076003, arXiv:2009.00017 [hep-th].

[69] I. Affleck, "On Constrained Instantons," *Nucl. Phys. B* **191** (1981) 429.